NMR Study of Antiferromagnetic α-Mn and β-Mn Alloys

Takao Kohara

March 1974

Synopsis

NMR study has been made on various antiferromagnetic α- and β-Mn alloys at liquid helium temperatures. The alloys used are α-Mn with V, Cr, Fe, Co, Ni, Ru, Re, Al and Zn impurities, and β-Mn with Ti, V, Cr, Fe, Co, Ni, Ru, Rh, Pd, Ir, Al, Si, Zn, Ga, Ge, In and Sb. The measurements in α-MnFe alloys show that Fe atoms occupy site IV and increase the magnetic moments of Mn atoms at every site. Similar behavior is observed in Co, Ni and Ru alloys. On the other hand, Cr or V atoms prefer either site I or one of site II, decreasing the magnetic moments of surrounding Mn atoms. The changes both of the internal fields of Mn^{55} and of T_N are explained by the occupation of sites by several impurity atoms. The changes of the lattice constant and of the average number of d-electrons have also an important effect to the magnetism of α-Mn alloys. Pure β-Mn metal is paramagnetic down to 1.1 K. Several β-Mn alloys become antiferromagnetic at 4.2 K by an addition of small amount of impurity metal. The internal field of Mn^{55} suggests that the magnetic moment on Mn is less than 0.5 μ_B. In β-MnCo alloys, the magnetic moment of Co is estimated to be about 1.0 μ_B. The magnetic ordering of β-Mn alloys with non-transition metal impurities is attributed to the increase of the lattice constant, which was measured by X-ray diffraction.

In the case of transition metal impurities, the lattice expansion, the change of the average number of d-electrons and the induction of the magnetic moments of Mn atoms by the localized moment on impurity atom must be considered.

CONTENTS

I. Introduction

In the study of electronic state in transition metals, the magnetic properties of manganese are of great interest. Mn^{55} nucleus has a natural abundance of 100 %, a spin I=5/2 and a comparatively large nuclear magnetic moment of 3.461 μ_N. Consequently, Mn^{55} is suitable for studying antiferromagnetic state in Mn alloys by nmr technique.

(1). Alpha-Mn has a body-centered cubic lattice with 58 atoms per cubic cell.[1] Several neutron diffraction investigations of α-Mn were performed.[2)-4)] These studies have reported that each of the four inequivalent sites has different magnetic moment, and have established the existence of antiferromagnetic state below 95 K. According to the neutron diffraction experiment by Yamada et al., the magnetic structure is described by a non-collinear configuration and the magnetic moments at site I, site II, site III and site IV are 1.9 μ_B, 1.7 μ_B, 0.6 μ_B and 0.2_5 μ_B, respectively.[4)] Moreover, the nmr signals of Mn^{55} at these sites under zero external field are observed, and the internal field at each site is determined.[5),6)] These values are given in Table I. It is considered from the several experimental results that localized magnetic moments exist on the Mn atoms at site I and site II above T_N, in marked contrast with the property of Cr metal, where the electrons are itinerant.

They are as follows: (a) the observation[7)] of distinct, temperature dependent nmr signal due to Mn at site I and site II,

exhibiting a maximum negative shift 5.85 %, and unshifted, temperature independent resonance due to Mn atoms at site III and site IV, (b) the observation of esr signal, of which the line width becomes drastically wider as the temperature approaches T_N,[8] (c) the large resistivity of α-Mn due to spin-disorder scattering process.[11] Any way, the magnetic properties of α-Mn are mainly determined by the Mn atoms at site I and site II.

Bellau and Coles[9] and Sato and Arrott[10] found that an addition of Fe to Mn raises Néel temperature while an addition of Cr to Mn suppresses it. By recent systematic resistivity studies,[11]-[13] it turned out that T_N of α-Mn alloys with a few at.% of Fe, Co, Ni or Ru, increases while T_N of the alloys with Cr or V decreases. On the other hand, Kimball et al.[14] and Kasper[15] have shown that the Fe atoms in α-Mn alloys preferentially occupy the definite sites by Mössbauer effect and neutron diffraction study in powdered sample, respectively. They analyzed from their results that relatively small atoms, such as Fe or Cr, occupy site III and site IV by the idea of space= filling. But this analysis seems not always perfect. To understand the change of T_N with the impurities, it is necessary to know which site the impurity atoms occupy.

The purpose of the present study is to clarify the occupation of four inequivalent sites by the impurity atoms, such as V, Cr, Fe, Co and Ni by observing the nmr signal of Mn^{55} in α-Mn alloys, and to know the change of the internal field at each site

with the impurity concentration. These nmr data on α-Mn alloys, conversely, may be useful for studying a detailed electronic state of pure α-Mn, which has a magnetically complicated structure.

(2). Beta-Mn has a simple cubic lattice with 20 atoms per unit cell[16] in which these atoms occupy two inequivalent sites as follows: 8 atoms in site I and 12 atoms in site II. The crystal structure is a little simpler than that of α-Mn. The neutron diffraction experiment by Kasper and Roberts[3] reported that β-Mn is neither ferromagnetic nor antiferromagnetic down to 4.2 K. Moreover, the nmr signal of Mn^{55} in β-Mn is also observed in usual resonance condition down to 1.1 K by the present experiment, which shows that pure β-Mn remains in paramagnetic state down to 1.1 K. On the other hand, the recent magnetization measurement[17] reports that β-MnCo alloys seem to show antiferromagnetic behavior at low temperature in the concentration range of less than 40 at.%Co.

The purpose of the present study is to investigate the magnetic properties of β-Mn alloys with various kinds of impurity elements by nmr technique, though there are little data of other experiments, such as neutron diffraction and electrical resistivity measurements.

II. Experimental procedures

(A). Sample preparation

The alloys used in this experiment were prepared by induction melting electrolytic Mn metal with impurity metal in appropriate concentration in corundum crucible under an atmosphere of pure argon. Purities of the metals are all more than 99.9 %.

Especially the alloys in the case of less than 1.0 at.% impurity concentration were made by the successive dilution of mother alloys with pure Mn. In the case the metals used were more than 99.995 % pure. To make α-phase alloys, the ingots were sealed in a quartz tube filled with argon gas at a pressure of 400 mmHg and annealed at 600°C for 45 hours. As to β-phase samples, the ingots in a quartz tube filled with purified argon gas at a pressure of 200 mmHg were kept at 950°C for 30 hours. These conditions are a little different according to the kind and the concentration of impurity elements. In some of α-Mn alloys, such as α-Mn 4 at.%Cr, two kinds of heat treatments were done to investigate the effect of heat treatment. For one alloy the temperature and the period of annealing were 600°C and 36 hours, respectively, while for another alloy they were 450°C and 100 hours, respectively. Any difference in nmr results was not observed between two kinds of alloys. To prepare the alloys of β-Mn, a rapid quenching, the ingot at the annealing temperature being dropped into ice water for less than one second, was performed. After these heat treatments, the ingots were crushed into powder in an agate mortar.

The sample size is smaller than 70 μ. The crystal structure

of these powdered samples was confirmed by X-ray diffraction. This method will be described in later part. Every time when the ingots were annealed for β-Mn alloys, the ingot of pure Mn was also sealed in a quartz tube together with the ingots of alloys separately on combustion boat. The effect of heat treatment was checked by observing the nmr signal of pure β-Mn.

(B). NMR method

1. The determination of the line shape

All the measurements were carried out by spin echo technique at liquid He temperature in zero external field. The equipments used in our nmr experiment were composed of high power pulsed oscillator and high sensitivity receiver with variable frequency from 4 MHz to 270 MHz. The line shape was determined by plotting versus frequency the amplitude of the spin echo signal which was obtained by first 90° and second 180° pulses. The interval of frequency was from 500 KHz to 2 MHz, and H_1 (rf field strength) was kept as constant as possible. The receiver system was of converter type above 16 MHz. In the frequency range of less than 17 MHz, the receiver of straight amplifier type was used.

Here the signal of Mn^{55} in pure β-Mn or Sn^{119} in pure Sn metal is used under an external field as a reference for sensitivity calibrator. When signals appear in widely distributed frequency range, we must consider the gain difference of equipments and other factors, such as the difference in Boltzmann factor, to obtain the true line shape. In order to eliminate these ambiguities

we used the signals of Mn^{55} at four sites in α-Mn.[6] We obtained the true line shapes using such correction that the integrated intensity ratio of these α-Mn signals becomes equal to the ratio of the atom number of the four sites. To investigate the change of the echo intensity with impurity concentration, the samples were treated under the same condition as possible, that is, the same weight and the same Q-value in a sample coil. The temperature was determined by the vapor pressure of liquid He. Spin echo amplitude depends on the separation between two pulses as

$$A=A_0\exp(-2\tau/T_2),$$

where τ is the separation time between two pulses, T_2 is the transverse relaxation time, and A is the observed echo amplitude. Echo amplitude extrapolated to $\tau=0$ is used to obtain the true echo intensity, because T_2 is different at each frequency. At the same time, T_2 was easily obtained by varing separation between two pulses.

The internal field was determined using the nuclear g-value of Mn^{55} of 10.500 MHz/10kOe,[18] and of Co^{59} of 10.054 MHz/10kOe.[19]

2. Investigation of magnetic ordering

When the substance become antiferromagnetic at liquid He temperatures, the nmr signal which appears in usual resonance condition at higher temperatures disappears under the same resonance condition and a signal is observed without external field. This occurrence of internal field is the evidence of the magnetic ordering. We determined the substance to be antiferromagnetic at 4.2 K

when the signal that appears at room temperature in usual resonance condition is lost at 4.2 K.

(C). X-ray diffraction technique

The X-ray measurements have been made on powdered samples of α-Mn alloys and β-Mn alloys in order to study the following problems.

[1]. Have the alloys with impurity elements in an appropriate concentration a definite phase perfectly?

[2]. If the change of interatomic distance between pure Mn and Mn alloys was observed, is this change related with the magnetic properties of these alloys?

A careful determination of the change of interatomic distance, $\Delta d/d$, in α-Mn alloys and β-Mn alloys was made by a standard diffractometer at room temperature employing a finely collimated beam of FeK_{α} radiation, and correcting the reflection angle with the reference specimen of Si. In these measurements, the samples were the same powdered ones as used in the nmr experiments. The changes of the lattice constants were almost the same in each alloy within the experimental error, and, therefore, no preferential orientation in the change of interatomic distance was assumed.

III. Experimental results and Discussions

(a). α-Mn alloys

1. The alloy with an impurity element of Fe, Ru, Co or Ni

Fig.1 shows the frequency distribution of the spin echo intensity of Mn^{55} at site I in pure α-Mn, 1 at.%Fe, 8 at.%Fe, 12 at.%Fe, 24 at.%Fe and 30 at.%Fe alloys at 4.2 K. The solubility limit of Fe in α-Mn is about 33 at.%.[20] The line shape is symmetric as to resonance frequency, and the internal field is evaluated from the peak frequency. The integrated intensity at site I is almost constant up to 30 at.%Fe concentration. The line shapes of Mn^{55} at site II and site III in the same sample are shown in Fig.2 and Fig.3, respectively. Also at these sites the intensities are almost constant with Fe concentration. As are seen in these figures, the line shapes are not symmetric.

The internal fields are therefore defined at the gravity points of the line shapes. At site IV in 24 at.%Fe and in 30 at.%Fe alloys, the intensities were reduced to about one third and about one fourth of the intensity in pure α-Mn or less than 4 at.%Fe alloys, respectively, as shown in Fig.4. From these nmr results, Fe atom is considered to prefer only site IV. This result is partially consistent with the result of Mössbauer effect experiment[14] and neutron diffraction studies,[15] which propose that Fe atoms occupy site III and site IV. Similar experiments were performed in the alloys up to 9 at.%Ru, 2 at.%Co and 2 at.%Ni.

The results are shown in Fig.5, Fig.6 and Fig.7. The solubility limit of Ru, Co and Ni are 12 at.%, 2 at.% and 2 at.%,

respectively.[20] Because of the small solubilities of these alloys, we could not make a precise measurement of the concentration dependence of the intensity in these alloys as in the case of Fe alloys. As the line shapes and the intensities of Mn^{55} at site I, site II and site III in α-Mn alloys with Ru, Co or Ni show similar behavior to those of α-MnFe alloys, Ru, Co or Ni atoms are considered to go into only site IV, or site IV and site III at least.

Fig.8 shows the concentration dependence of the internal field in α-MnFe alloys and α-MnRu alloys at site I, site II and site III.

The internal fields at site I, site II and site III increase with the concentration of impurity such as Fe or Ru, suggesting that the magnetic moments at these sites increase. Consulting the ratio of the internal field to magnetic moment in pure α-Mn,[6] one can estimate the rates of increase to be 0.02 μ_B/at.%Fe, 0.07 μ_B/at.%Fe and 0.04 μ_B/at.%Fe at site I, site II and site III, respectively.

The rate in α-MnRu alloys is more than that in α-MnFe alloys.

Thus Fe, Ru, Co and Ni atoms enter the non-magnetic sites and increase the moments of surrounding Mn atoms. Fig.12 shows the increase of the internal field at site I with the impurity concentration. As to the increase of the internal field at Mn^{55}, the effect of Ru is largest.

2. The alloy with an impurity element of Cr or V

In Fig.9, the line shapes of Mn^{55} at site I and site II in α-MnCr alloys at 1.4 K are shown. The intensities of the signals at both sites decrease rapidly with Cr concentration and the signal at site I disappears in α-Mn 4 at.%Cr alloy. Fig.10 shows the

dependence of the integrated intensity on the concentration in various kinds of alloys. An apparent increase of the integrated intensity in the alloy with 1 at.% impurity compared with that in α-Mn is attributed to the inevitable change of the Q-value of a sample coil which may come from the difference of the brittleness of the alloys. On the other hand, the intensity of the signals appearing at frequencies corresponding to site III and site IV increase and the line shapes become wider with Cr concentration.

The experiments on α-MnV alloys are also performed in the alloys up to 4 at.%V which give similar results to α-MnCr alloys. These results are shown in Fig.10. The result suggests that Cr or V atoms enter either site I or one of site II. The magnetic moments at site I and site II surrounding Cr atoms are reduced largely, and their magnitudes become comparable with those of site III and site IV. The inference above to the occupation of Cr and V atom is supported by the following experiment. Similar measurements have been made in the ternary alloy systems, such as α-Mn 3.0 at.%Cr 1.92 at.%Co, where T_N's in the alloys are expected to be equal to that in pure metal. Fig.11 shows the intensity distribution at site I. As are seen in (a-3) and (b-3) of Fig.10, the decrease of the intensities at site I and site II in these ternary alloys are similar to that of α-MnCr alloys, but the peak position of the broad line shape does not shift. The fact that the intensity still decreases though the decrease of the moments is compensated suggests that the impurity atoms occupy site I or site II. Similar behavior is also observed in α-MnCrFe alloys and in α-MnCrRu alloys.

Fig.12 shows the shift of resonance frequency of Mn^{55} at site I in α-Mn alloys with the concentration of several kinds of impurity elements. As seen in Fig.13, this shift is reasonable compared with the change of T_N in the electrical resistivity measurements by Williams et al.[11] and Whittaker et al.[12] except for that of α-MnRu alloys. Any way, the magnetic property of α-Mn seems to be mainly determined by the Mn atoms at site I, though this site corresponds to only a few at.% at the most.

3. The alloy with an impurity element of Al, Zn or Re

We made the experiment in the alloys with Al, Zn and Re up to 3 at.%, 2 at.% and 5 at.%, respectively. No measurement of T_N is reported in these alloys. Fig.14 shows the line shapes of these alloys. The peak position of the line shape at each site in the alloys with Al, Zn and Re is almost same as that in pure α-Mn. The intensities at site I and site II decrease with Al concentration, and the intensities at site I and site II decrease with Re concentration as are shown in (a-4), (b-4), (a-5) and (b-5) of Fig.10. From these figures, Al atom seems to occupy site I mainly, and Re atom occupies both site I and site II. This result of Re alloys is consistent with the X-ray experiment by Ageev et al.[21] In the alloys with less than 2 at.%Zn, only a little broadening of the resonance line is observed. From the results, T_N's of these alloys seem not to change largely.

Fig.15 shows the change of the interatomic distance with the concentration of several kinds of impurity atoms by X-ray diffraction at room temperature. Here the marks ● and ○ show the

substances which have larger and smaller value of T_N compared with that in pure α-Mn metal, respectively.

From our nmr experiments, it becomes clear that the following three points are important.

[1]. The occupation of site by the impurity atom.

As already discussed, Cr and V atoms enter the magnetic sites and destruct the moments of surrounding Mn atoms giving rise to the decrease of T_N.

[2]. The number of d-electrons.

Though Fe, Ru, Co and Ni atoms enter non-magnetic sites, they increase T_N. The number of d-electrons seems to play an important role. This is partially supported by the change of T_N per 1 at.% of several kinds of impurity shown in Fig.16.

[3]. Lattice change.

As in the case of β-Mn alloys discussed in the following section, the lattice expansion is an important origin for the increase of magnetic moment on Mn atoms. The fact that Ru has larger effect on the increase of T_N than Fe, both of which have equal number of d-electrons, is attributed to this lattice change shown in Fig.15. In spite of the occupation of magnetic sites by Al or Re atoms with no magnetic moment, no shift of nmr frequency of Mn^{55} at each site is observed in the present experiment. This seems to be due to the compensation of the destruction of magnetic moment on Mn by the increase of the moment caused by the lattice expansion.

(b). β-Mn alloys

Table II shows the results for β-Mn alloys with several kinds of impurities. Here the number shows the concentration (at.%) of impurities. In the concentration range of impurity element indicated in brackets, the alloys are in paramagnetic state at 4.2 K. In the concentration range shown in parentheses, the alloys show antiferromagnetism at 4.2 K. All the alloys studied are paramagnetic at 77 K, except for the alloys with more than 15 at.%Co alloys.

1. Transition metal impurity

As are seen in Table II, the alloys with impurity elements, such as Ti, V and Cr which have less 3d-electrons than Mn, do not show any magnetic ordering even at 4.2 K, while the alloys with impurities which have more than 3d-electrons than Mn show antiferromagnetism. Fig.17 shows the line shapes for Mn^{55} and Co^{59} in β-MnCo alloys at 1.4 K. The integrated intensity of the higher frequency part in Fig.17 is shown in Fig.18. The signals of higher and lower frequency parts are attributed to Co^{59} and Mn^{55}, respectively. The change of the internal field of Co^{59} with Co concentration is shown in Fig.19. The magnetic moment of Co is rather larger than that of Mn and is estimated to be more than 1 μ_B. Fig.20 shows the concentration dependence of the internal field at Mn^{55} for various kinds of alloys. As the internal fields at Mn^{55} in antiferromagnetic Mn alloys are reported to be about 80 kOe/μ_B in the previous works,[6),22)] the magnitude of the moments in the alloys of the present experiment is estimated to be less than 0.5 μ_B. As shown in Fig.20, Ir

alloy seems to have the largest moment. If we compare the internal fields of Mn^{55} in Fe, Co and Ni alloys, Ni alloy has the biggest and Fe alloy has the smallest moment. This order is consistent with the recent work on the magnetization measurement by Hori in those three alloys,[23] where Ni and Fe alloys are reported to have the biggest and the smallest moments, respectively. In Fig.21, the change of the lattice constant by X-ray diffraction at room temperature is shown against the concentration of several transition impurities. Here the mark ● shows the substance which becomes antiferromagnetic at 4.2 K and the mark O shows the substance which remains in paramagnetic state at 4.2 K. In this figure, with one exception of Fe alloys, all the alloys become antiferromagnetic when the lattice spacing increases. Especially, the increase of the lattice constant is remarkable in Ni, Ir and Ru alloys which have the large internal fields at Mn^{55}. Therefore, we conclude that one of the important origins of the magnetic ordering in β-Mn alloys with transition impurities is the expansion of the lattice spacing. This mechanism plays an important role in the occurrence of magnetic ordering in β-Mn alloys with non-transition metal impurity and is discussed in the following part.

As already mentioned, Fe alloys show antiferromagnetic behavior, though the lattice constant decreases. Therefore, we must consider the role of localized moment on impurity atom and/or the change of the average number of d-electrons. In the former case, a localized magnetic moment associated with impurity atom polarizes the moments of the surrouning Mn atoms just

like the case in ferromagnetic Pd-Co alloys. Rather large magnetic moments estimated on Co atoms make this consideration reasonable. In the latter case, the effect of the number of d-electrons must be considered like in the case of α-MnFe alloys, where Fe atoms increase the magnetic moments on Mn atoms though Fe atoms occupy the non-magnetic sites. To investigate this point, we prepared the following alloy system so as to control the number of d-electrons. The results obtained by nmr at 4.2 K are as follows:

$Mn_{96}V_2Fe_2$	(L)------para,
$Mn_{98}Re_2$	(E)------para,
$Mn_{96}Cr_2Fe_2$	(E)------para,
$Mn_{96}Cr_2Co_2$	(M)------antiferro,
$Mn_{86}V_4Co_{10}$	(M)------antiferro,
$Mn_{86}Cr_4Co_{10}$	(M)------antiferro,
$Mn_{81}Cr_4Co_{15}$	(M)------antiferro.

Here the substances with the notation, L, M and E have the d-electron number less than, more than and equal to that in Mn on the average, respectively. A close correlation between the magnetic ordering and the number of d-electrons in this table indicates the importance of the number of d-electrons. Fig.22 shows the change of the lattice constant in the ternary alloys. The change of the lattice constant has no correlation with magnetic ordering so far as these alloys are concerned. Here the effect of the localized moments must also be considered as well. The signals of Co^{59} in the ternary β-Mn 4 at.%Cr 10 at.%Co, was also observed.

In the ternary alloys the internal fields both of Co^{59} and of Mn^{55} become somewhat smaller than in the binary β-Mn 10 at.%Co

alloy. That is if the magnetic moments of Mn are induced by an addition of Fe or Co etc. which may have localized magnetic moment, both magnetic moments of Co and the induced magnetic moments of Mn are considered to be destructed by the third element, such as Cr or V. Furthermore, as seen in Fig.20, Ir alloys have larger magnetic moments than Sb alloys although the lattice expansion rates of these alloys are almost same from Fig.21 and Fig.24. This indicates the importance of the number of d-electrons.

Thus the next three mechanisms must be considered in order to understand the magnetic behavior of β-Mn alloys with transition impurities. They are as follows:

[1] The lattice expansion mechanism.

[2] The possibility of induced magnetic moment of Mn due to the localized magnetic moments of impurity atoms, such as Co.

[3] The number of d-electrons.

The transverse relaxation time, T_2, of Co^{59} in β-MnCo alloys at 1.4 K is shown in Fig.23. T_2 drastically decreases with the decrease of Co concentration. As T_2 of Co^{59} is temperature dependent, T_1 (the longitudinal relaxation time) process mainly contributes to T_2. The decrease of T_1 is considered to be due to the slowing down of the spin fluctuation with the decrease of Co concentration. On the other hand, T_2 of Mn^{55} measured in pure β-Mn metal and in 5 at.%Co, 10 at.%Co and 20 at.%Co alloys at 1.4 K does not show any such drastical change. It increases almost

linearly from 110 μsec., in pure β-Mn, to 130 μsec., in 35 at.%Co alloy. The values of T_2 of Mn^{55} in antiferromagnetic alloys with a few at.% of several impurities are almost equal to that in pure β-Mn metal.

2. Non-transition metal impurity

In the same way as in the alloys with transition metal impurity, β-Mn alloys with non-transition metal impurities are also divided according to the paramagnetic character and the antiferromagnetic one, and are listed on the right hand part of Table II.

The internal fields of Mn^{55} in β-Mn alloys containing In and Al are shown in Fig.20. The magnitudes of magnetic moments on Mn atoms are estimated to be less than 0.4 μ_B. Fig.24 shows the change of the interatomic distance with the concentration of several kinds of non-transition impurity elements by X-ray diffraction at room temperature. The alloys indicated by the mark ● become antiferromagnetic at 4.2 K. The alloys with the mark ○ remain in paramagnetic state at 4.2 K. Except for Si, all the impurities give rise to the increase of the lattice constant and when the interatomic distance increase more than 0.1 % the alloys enter antiferromagnetic state at 4.2 K without exception. Furthermore, In alloy of which the lattice expansion is the largest of all alloys containing non-transition impurities, has the largest internal field as shown in Fig.20. The internal field of Mn^{55} in β-Mn 4 at.%Al is lower than those in In and Sb alloys. Thus the expansion of the lattice constant is concluded to be the main origin

of the magnetic ordering. This importance is predicted previously by Yamada in the discussion of the magnetism of α-, β- and γ-Mn.[4),24)] According to Moriya's theory,[25)] when there is a pair of atoms of the same kind in metal, the critical boundary for the appearence of the localized magnetic moment is as follows:

[1] The condition for the appearence of ferromagnetic coupling is

$$(U+4J)/\Delta > \pi\{1+(V/\Delta)^2\} .$$

[2] The condition for the appearence of antiferromagnetic coupling is

$$(U+4J)/\Delta > \pi\{(V/\Delta)/\tan^{-1}(V/\Delta)\} .$$

Here Mn atom has five 3d-electrons, and U and J are the intra=atomic Coulomb and exchange energies, respectively, Δ is the width of the virtual level due to s-d mixing, V is the transfer integral of d-electrons in atomic pairs, and depends on the lattice constant.

These conditions are shown in Fig.25 which is cited from ref.24.

Keeping U, J and Δ to be constant, magnetic ordering breaks down when V goes over a critical value. In pure β-Mn, V is considered to be too large and the condition [2] is not fulfilled. By the introduction of impurities, V decreases with the increase of the lattice spacing. Then the condition [2] is finally fulfilled and the antiferromagnetic ordering appears.

At any rate, more experimental results, such as the neutron diffraction, the electrical resistivity measurement and the Mössbauer effect, are expected in order to discuss the magnetism of β-Mn and β-Mn alloys precisely. Furthermore, the theoretical problem of β-Mn alloys remains to be solved.

IV. Conclusion

(1). α-Mn alloys

Fe atoms occupy only site IV, increasing the magnetic moments of Mn at every site. Ru, Co or Ni atoms which give similar effects as Fe, enter neither site I nor site II.

Cr atoms enter site I or one of site II, reducing the magnetic moments of Mn surrounding Cr. Similar behavior is also observed in α-MnV alloys. Al atoms seem to prefer site I, and Re atoms enter site I and site II at least. Any shift of nmr frequency of Mn^{55} is not observed in Al, Re and Zn alloys.

In the study of the magnetism of α-Mn alloys, we must consider the definite occupation of sites by impurity atoms, the average number of d-electrons and the change of interatomic distance.

(2). β-Mn alloys

β-Mn alloys with small amount of non-transition element, such as Al, Zn, Ga, Ge, In and Sb, become antiferromagnetic at 4.2 K, when the lattice expansion goes over 0.1 % at room temperature. The increase of the lattice constant is a main origin for magnetic ordering. β-Mn alloys with small amount of transition element, such as Fe, Co, Ni, Ru, Rh and Ir, become antiferromagnetic at 4.2 K. In this case not only the lattice expansion but the change of the average number of d-electrons and the existence of localized moments on impurity atoms play an important role.

Acknowledgements

The author would like to express his sincere thanks to Professors J.Itoh and K.Asayama for their continuous guidances and encouragements. He is also indebted to Dr. H.Takenaka and Dr. H.Yamagata for their advices and discussions. Thanks are also due to Professor T.Yamada and Dr. K.Terakura for their discussions.

References

1). A.J.Bradley and J.Thewlis: Proc.Roy.Soc. A115 (1927) 456.

2). C.G.Shull and M.K.Wilkinson: Rev.Mod.Phys. 25 (1953) 100.

3). J.S.Kasper and B.W.Roberts: Phys.Rev. 101 (1956) 537.

4). T.Yamada, N.Kunitomi, Y.Nakai, D.E.Cox and G.Shirane: J.Phys.Soc.Japan 28 (1970) 615.

5). J.Itoh, Y.Masuda, K.Asayama and S.Kobayashi: J.Phys.Soc.Japan 18 (1963) 455.

6). H.Yamagata and K.Asayama: J.Phys.Soc.Japan 33 (1972) 400.

7). V.Jaccarino and J.A.Seitchick: Bull.Amer.Phys.Soc. 10 (1965) 317.

8). T.Kohara, Y.Oda and K.Asayama: in preparation.

9). R.V.Bellau and B.R.Coles: Proc.Phys.Soc. 82 (1963) 121.

10). H.Sato and A.Arrott: J.Phys.Soc.Japan Suppl. 17 (1962) 147.

11). W.Williams Jr. and J.L.Stanford: Phys.Rev. B7 (1973) 3244.

12). K.C.Whittaker and P.A.Dziwornooh: J.Low Temp.Phys. 5 (1971) 447.

13). Y.Nakahashi, T.Yamaoka, M.Mekata and H.Takagi: Annual Meeting of the Physical Society of Japan (1972).

14). C.W.Kimball, W.C.Phillips, M.V.Nevitt and R.S.Preston: Phys.Rev. 146 (1966) 375.

15). J.S.Kasper: Theory of Alloy Phases (American Society of Metals, Cleveland, Ohio, 1956), p.264.

16). G.D.Preston: Phil.Mag. 5 (1928) 1207.

17). T.Hori: Annual Meeting of the Physical Society of Japan (1973).

18). W.B.Mims, G.E.Devlin, S.Geschwind and V.Jaccarino: Phys.Letters 24A (1967) 481.

19). R.E.Walstedt, J.H.Wernick and V.Jaccarino: Phys.Rev. 162 (1967) 301.

20). M.Hansen: Constitution of Binary Alloys (McGraw-Hill Book Company, Inc., New York, 1958).

21). N.V.Ageev and V.Sh.Shekhtman: Dok.Acad.Nauk 143 (1962) 922.

22). H.Takenaka and K.Asayama: J.Phys.Soc.Japan 35 (1973) 740.

23). T.Hori: private communication.

24). T.Yamada and N.Kunitomi: Bussei 5 (1971) 249 [in Japanese].

25). T.Moriya: Progr.Theor.Phys. 33 (1965) 157 ; Proc. International School of Physics "Enrico Fermi" Course 37, (Academic Press, 1967) p.206.

Figure Captions

Fig.1. The line shapes of Mn^{55} at site I in pure α-Mn and in α-MnFe alloys: 1, 8, 12, 24 and 30 at.%Fe measured at 4.2 K.

Fig.2. The line shapes of Mn^{55} at site II in pure α-Mn and in α-MnFe alloys: 1, 8, 12, 24 and 30 at.%Fe measured at 4.2 K.

Fig.3. The line shapes of Mn^{55} at site III in pure α-Mn and in α-MnFe alloys: 1, 8, 12, 24 and 30 at.%Fe measured at 4.2 K.

Fig.4. The line shapes of Mn^{55} at site IV in pure α-Mn and in α-MnFe alloys: 1, 24 and 30 at.%Fe measured at 4.2 K.

Fig.5. The line shapes of Mn^{55} at site I in α-Mn alloys: 1 and 2 at.%Co; 1 and 2 at.%Ni; 1, 3 and 9 at.%Ru measured at 4.2 K.

Fig.6. The line shapes of Mn^{55} at site II in α-Mn alloys: 1 and 2 at.%Co; 1 and 2 at.%Ni; 1, 3 and 9 at.%Ru measured at 4.2 K.

Fig.7. The line shapes of Mn^{55} at site III in α-Mn alloys: 1 and 2 at.%Co; 1 and 2 at.%Ni; 1, 3 and 9 at.%Ru measured at 4.2 K.

Fig.8. Impurity concentration dependence of the internal fields of Mn^{55} in α-MnFe alloys and in α-MnRu alloys.

Fig.9. The line shapes of Mn^{55} at site I and site II in α-MnCr alloys: 1, 2 and 4 at.%Cr measured at 1.4 K. The scales of the intensity are different for site I and site II.

Fig.10. Integrated intensities of Mn^{55} signals at site I and site II in α-MnCr, α-MnV, α-MnCrCo, α-MnAl and α-MnRe alloys. In α-MnCrCo alloys, abscissa shows the concentration of Cr. The ratio of Cr and Co is always kept 1:0.64.

Fig.11. The line shapes of Mn^{55} at site I in α-MnCrCo alloys measured at 1.4 K.

Fig.12. Concentration dependence of the shift of Mn^{55} signal at site I in various α-Mn alloys.

Fig.13. Néel temperature in α-Mn alloys as a function of the impurity concentration. Fe_A and Fe_B are samples of Whittaker and Dziwornooh annealed at 620°C, and heated to 900°C and then annealed at 620°C, respectively. This result is adopted from ref.11.

Fig.14. The line shapes of Mn^{55} at site I and site II in α-Mn alloys: 1 and 3 at.%Al; 2 at.%Zn; 1, 3 and 5 at.%Re measured at 1.4 K. The scales of the intensity are different for site I and site II.

Fig.15. Relative change of the interatomic distance in α-Mn alloys at room temperature with the concentration of impurity.

Fig.16. The change of Néel temperature per 1 at.% of impurity concentration. These results are adopted from ref.11 and ref.13. The mark [O] shows the value in Ru alloy.

Fig.17. The line shapes of Mn^{55} and Co^{59} in β-MnCo alloys at 1.4 K. The scales of the intensity are different for Mn^{55} and Co^{59}.

Fig.18. Concentration dependence of integrated intensity of Co^{59} in β-MnCo alloys.

Fig.19. Internal fields of Co^{59} in β-MnCo alloys.

Fig.20. Internal fields of Mn^{55} in several β-Mn alloys.

Fig.21. Relative change of the interatomic distance in β-Mn alloys with several transition impurities at room temperature.

Fig.22. Relative change of the interatomic distance in ternary β-Mn alloys at room temperature.

Fig.23. T_2 of Co^{59} as a function of Co concentration at 1.4 K.

Fig.24. Relative change of interatomic distance in several β-Mn alloys with non-transition impurity at room temperature.

Fig.25. The critical boundary for the appearence of the localized magnetic moment versus V (transfer integral) of d-electrons in atomic pairs. Ferromagnetic coupling appears in the range of A, and antiferromagnetic coupling appears in the range of A and B.

Table I. The number of Mn atoms, the magnetic moment of Mn and the internal field at Mn^{55} at each site in α-Mn metal.

Site	No. of Atoms	at.%	Magnetic Moment (μ_B)	Internal Field of Mn^{55} (kOe)
I	2	3.45	1.9	189.9
II	8	13.79	1.7	144.3 137.6
III	24	41.38	0.6	29.5 25.2
IV	24	41.38	0.2_5	7.1 4.8

Table II. The magnetic property of several β-Mn alloys. The numbers indicate the concentration of impurities in at.%. In the concentration ranges shown in brackets and in parenthese, the alloys are in paramagnetic and in antiferromagnetic states at 4.2 K, respectively.

							Al [2] (3-4)	Si [3]	
							Zn [3] (5-7)	Ga (3)	Ge (3)	
Ti [2]	V [2-4]	Cr [2-4]	Mn	Fe [1] (2-20)	Co [0.1-0.5] (0.7-35)	Ni (0.5-12)				
				Ru (1-4)	Rh (2)	Pd (1)		In (3)		Sb (3)
			Re [2]		Ir (1-2)					

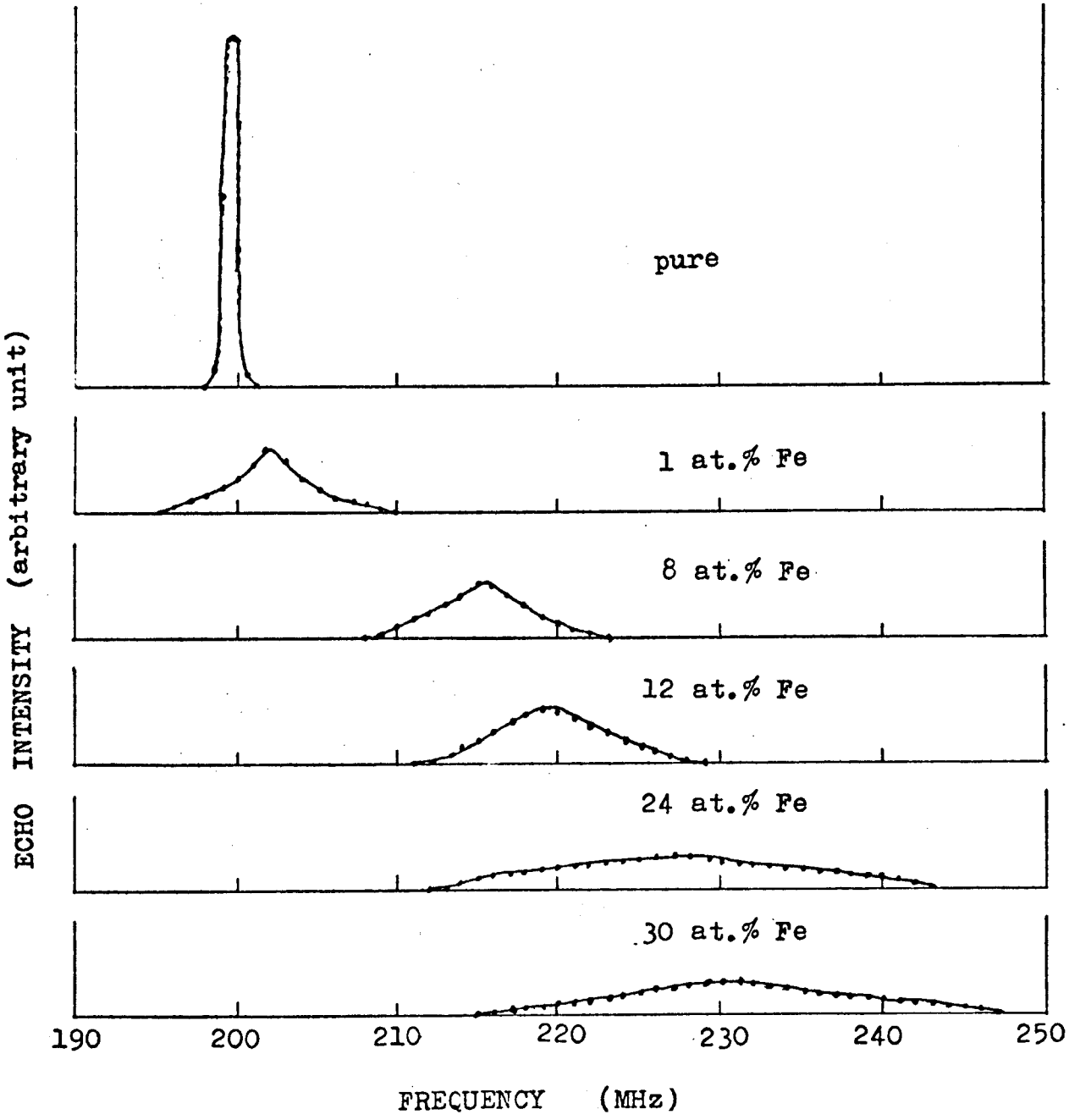
pure
1 at.% Fe
8 at.% Fe
12 at.% Fe
24 at.% Fe
30 at.% Fe
ECHO INTENSITY (arbitrary unit)
190
200
210
220
230
240
250
FREQUENCY (MHz)

Fig. 1

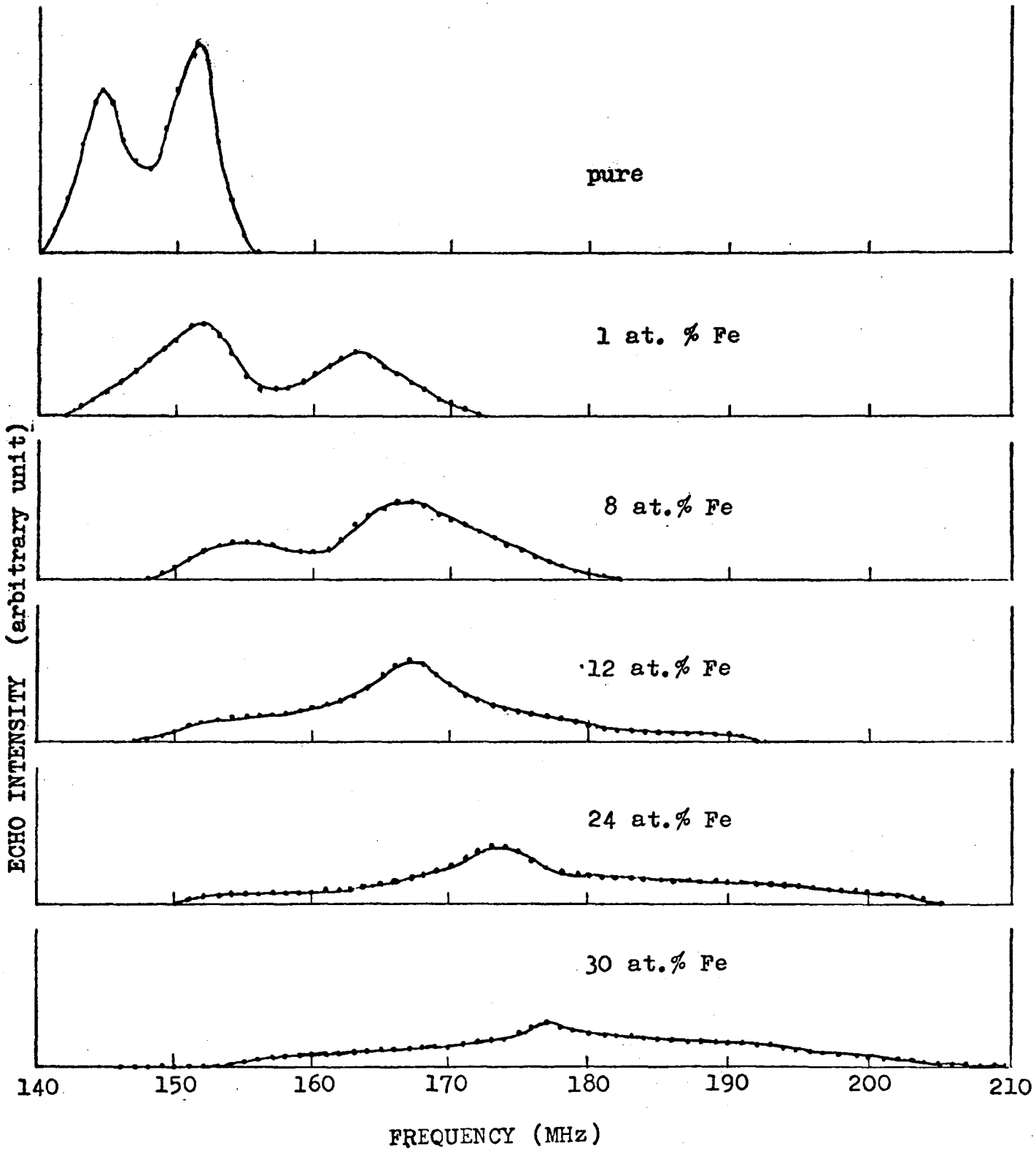
pure
1 at. % Fe
8 at.% Fe
12 at.% Fe
24 at.% Fe
30 at.% Fe
ECHO INTENSITY (arbitrary unit)
140
150
160
170
180
190
200
210
FREQUENCY (MHz)

Fig. 2

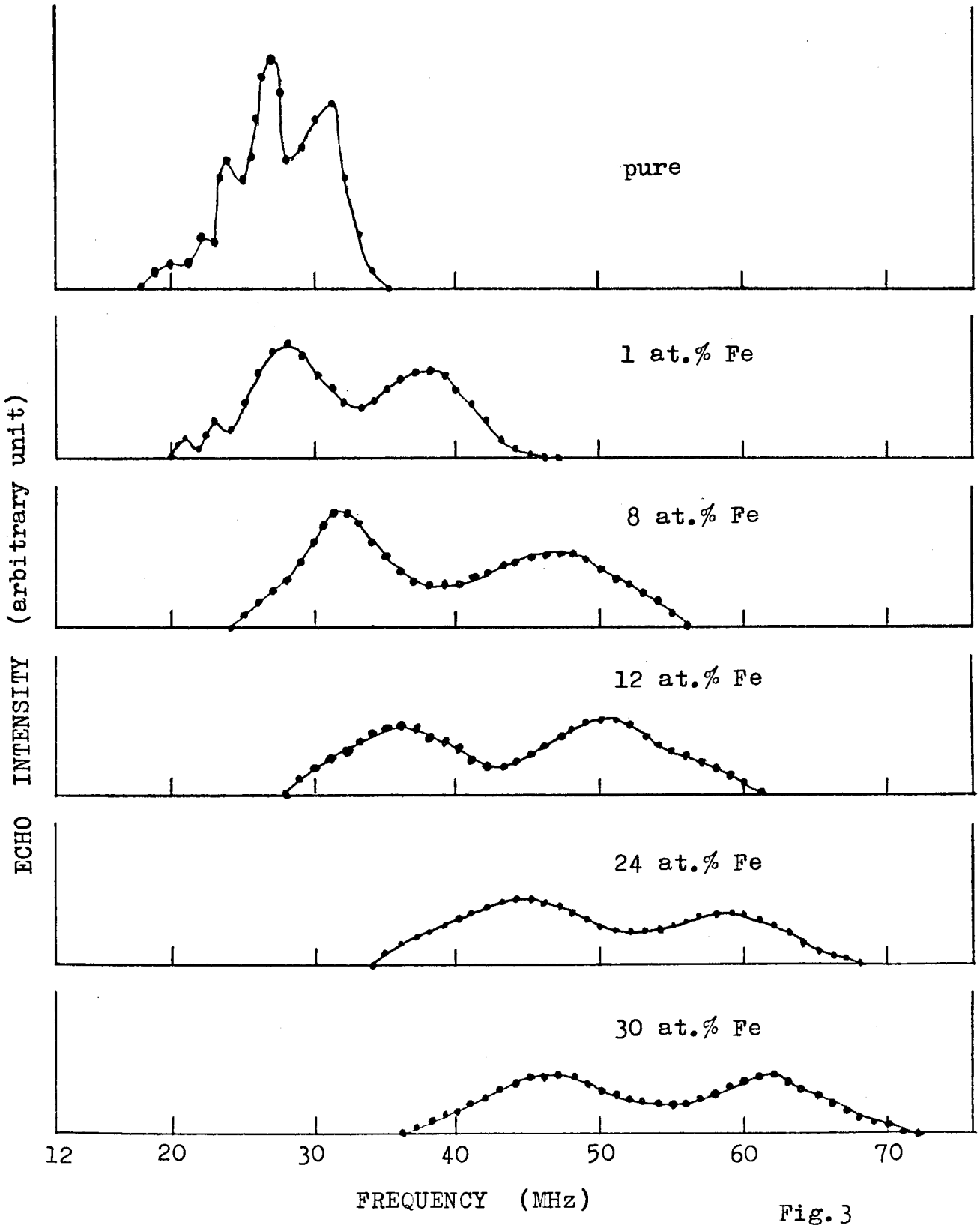
pure
1 at.% Fe
8 at.% Fe
12 at.% Fe
24 at.% Fe
30 at.% Fe
ECHO INTENSITY (arbitrary unit)
12
20
30
40
50
60
70
FREQUENCY (MHz)

Fig. 3

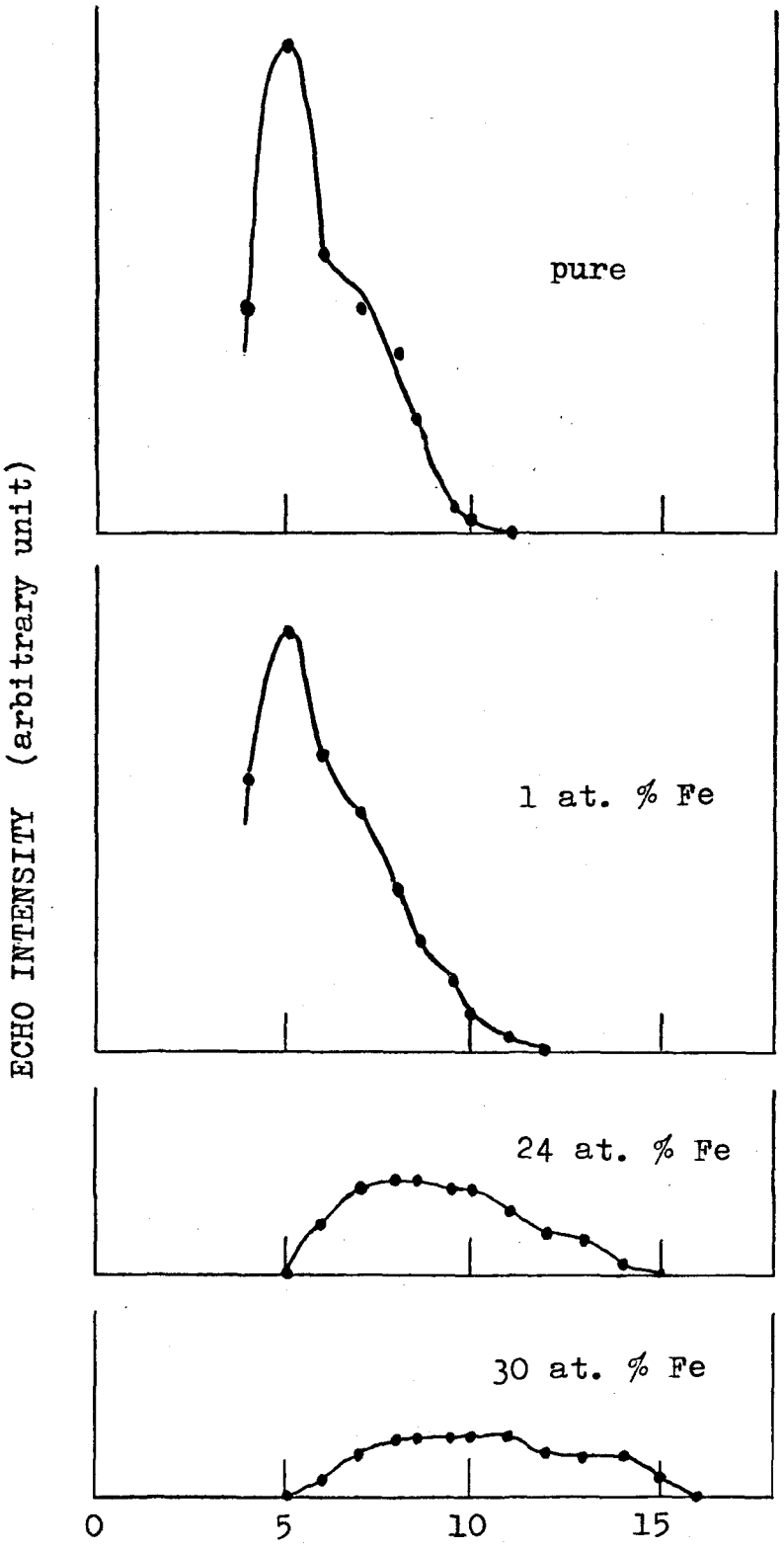
pure
1 at. % Fe
24 at. % Fe
30 at. % Fe
ECHO INTENSITY (arbitrary unit)
0
5
10
15
FREQUENCY (MHz)

Fig. 4

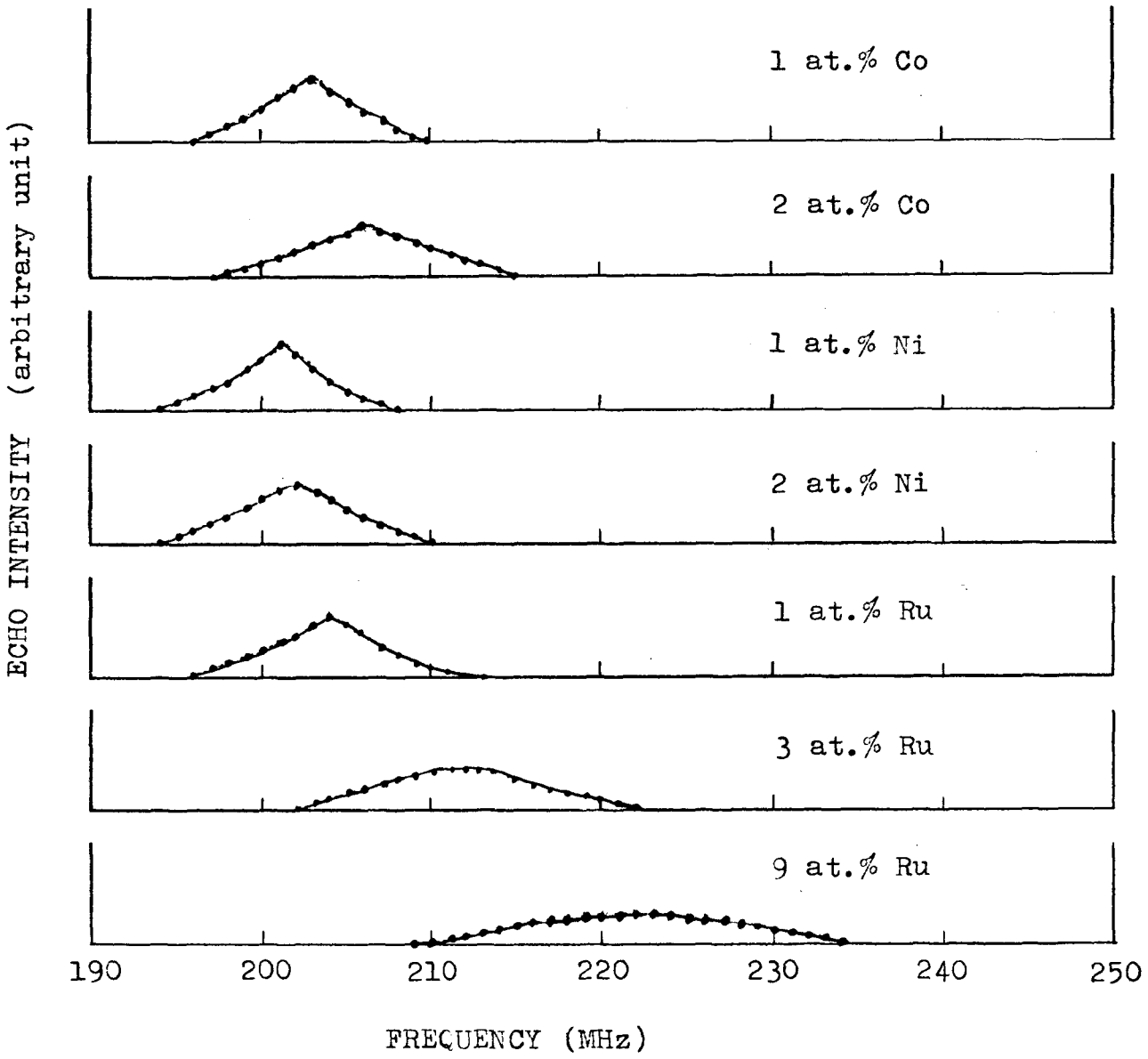
1 at.% Co
2 at.% Co
1 at.% Ni
2 at.% Ni
1 at.% Ru
3 at.% Ru
9 at.% Ru
ECHO INTENSITY (arbitrary unit)
190
200
210
220
230
240
250
FREQUENCY (MHz)

Fig. 5

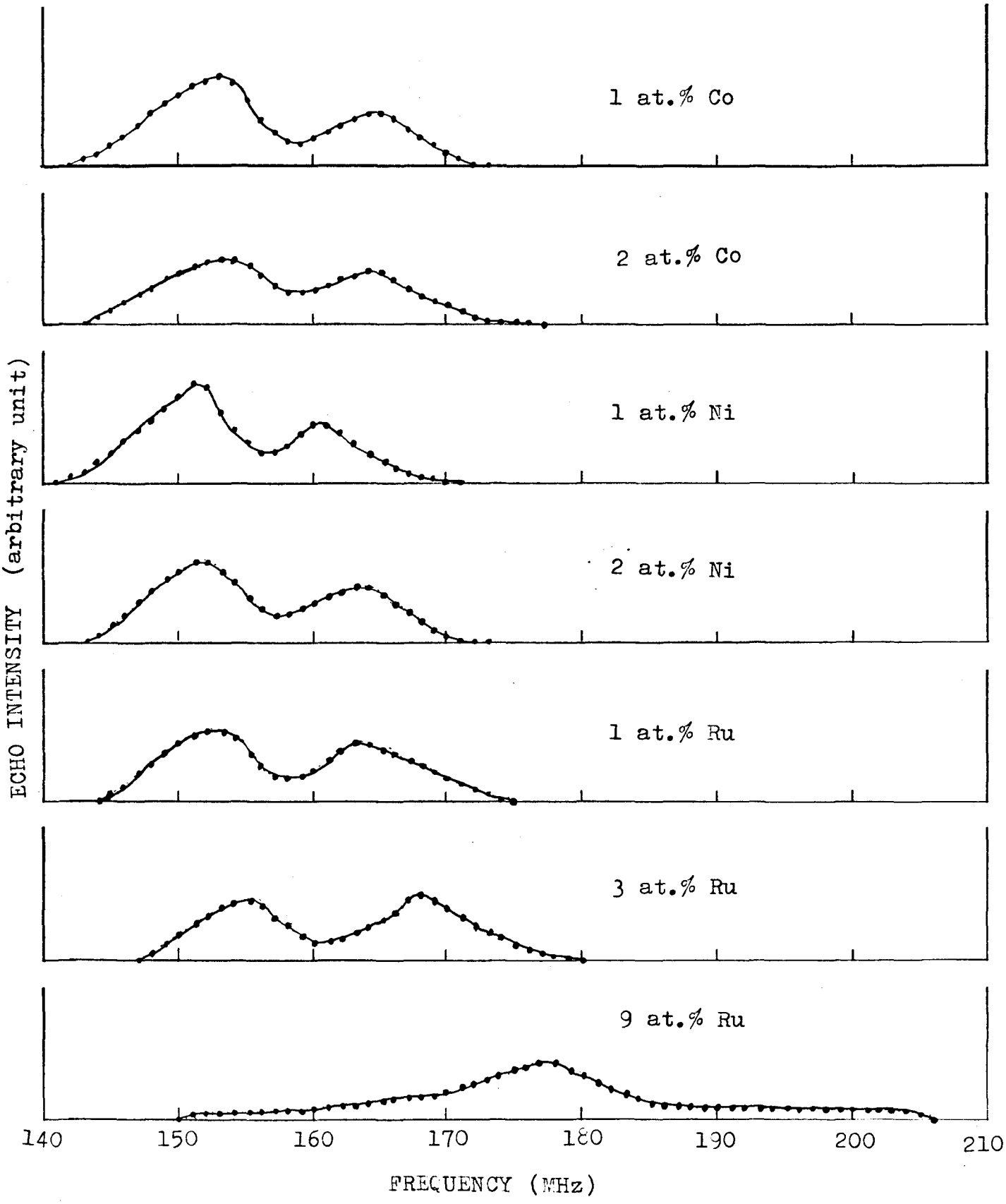
1 at.% Co
2 at.% Co
1 at.% Ni
2 at.% Ni
1 at.% Ru
3 at.% Ru
9 at.% Ru
ECHO INTENSITY (arbitrary unit)
140
150
160
170
180
190
200
210
FREQUENCY (MHz)

Fig. 6

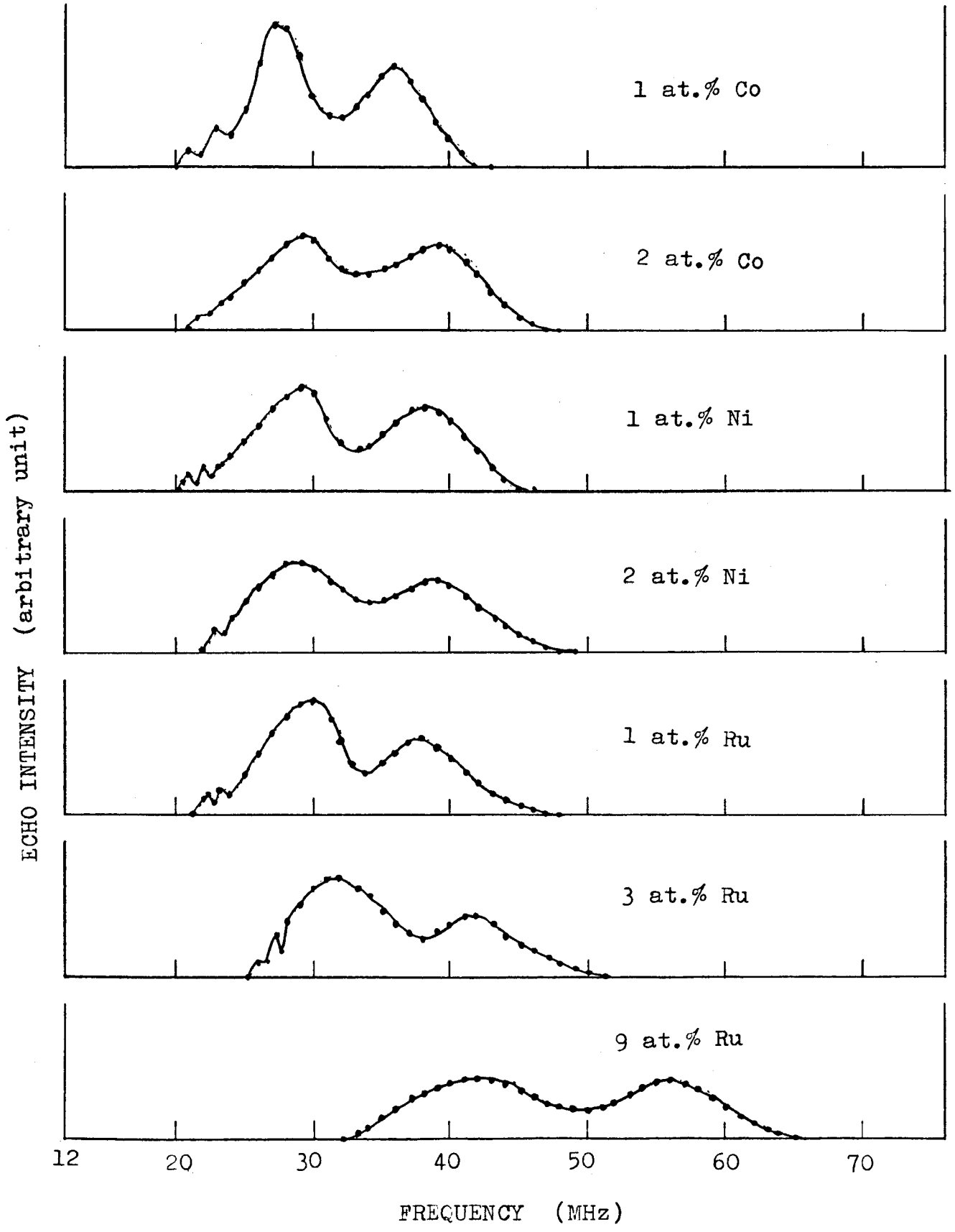
1 at.% Co
2 at.% Co
1 at.% Ni
2 at.% Ni
1 at.% Ru
3 at.% Ru
9 at.% Ru
ECHO INTENSITY (arbitrary unit)
12
20
30
40
50
60
70
FREQUENCY (MHz)

Fig. 7

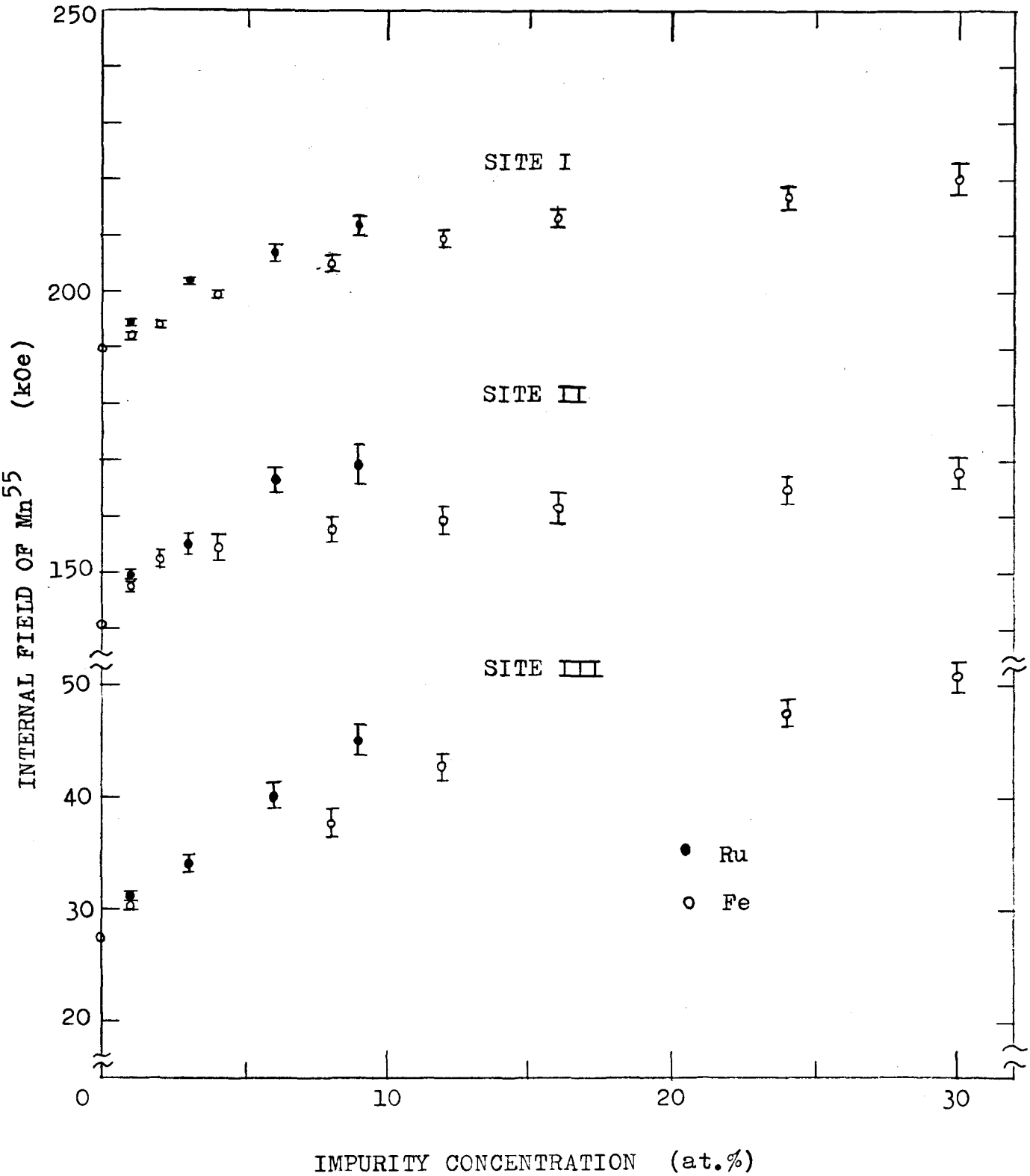
250
200
150
50
40
30
20
0
10
20
30
SITE I
SITE II
SITE III
Ru
Fe
INTERNAL FIELD OF Mn^{55} (kOe)
IMPURITY CONCENTRATION (at.%)

Fig. 8

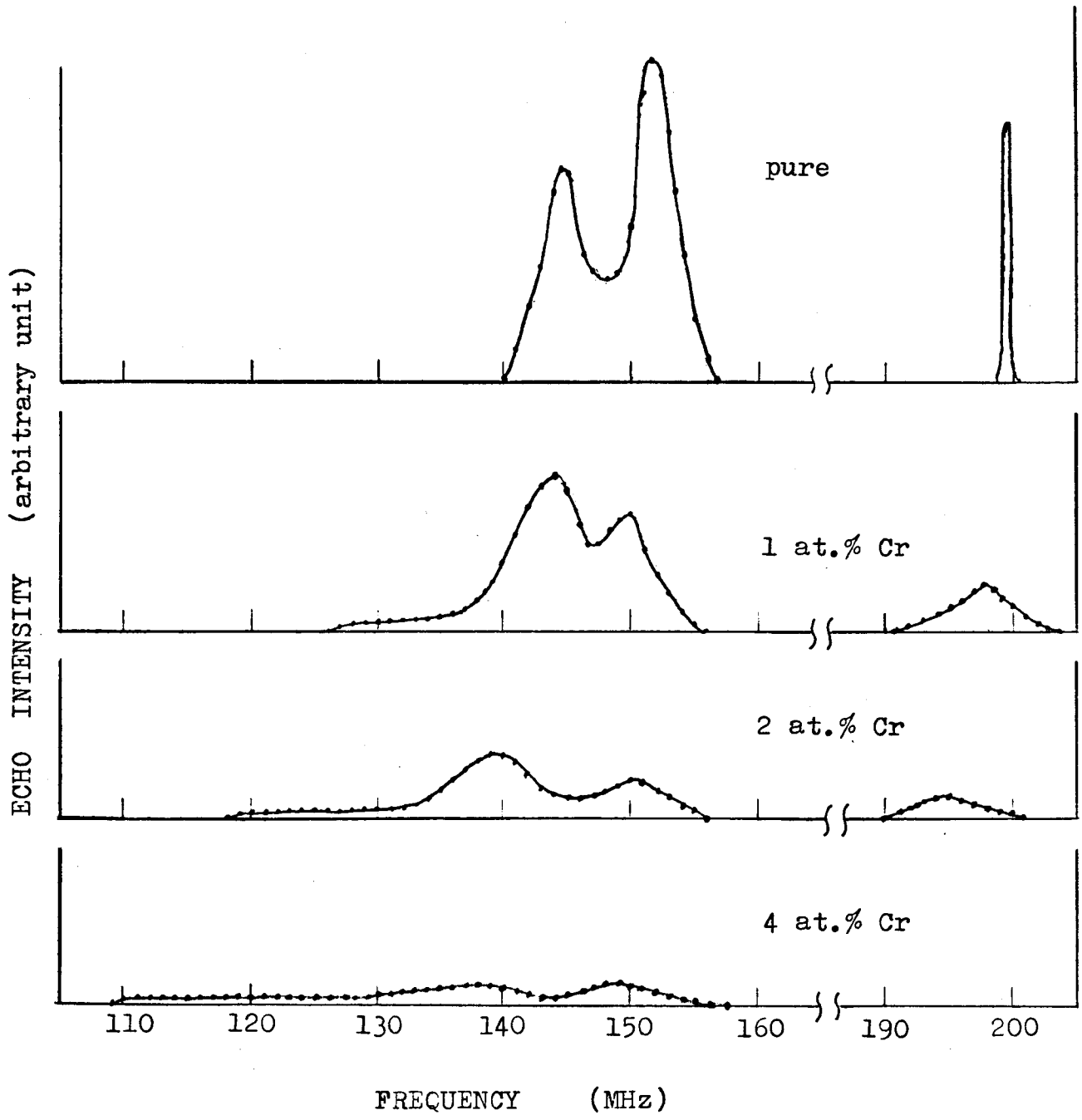
pure
1 at.% Cr
2 at.% Cr
4 at.% Cr
ECHO INTENSITY (arbitrary unit)
110
120
130
140
150
160
190
200
FREQUENCY (MHz)

Fig. 9

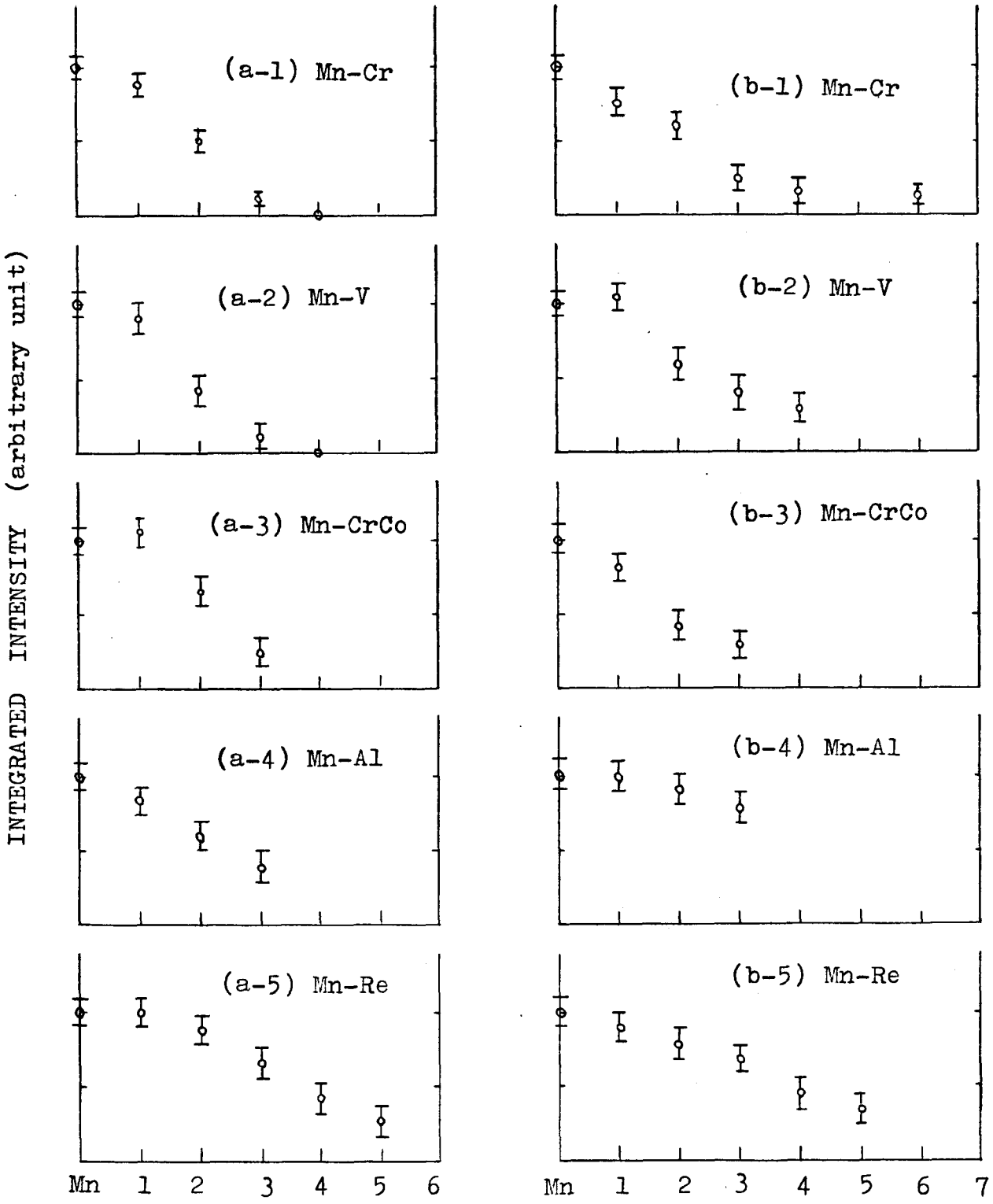
(a-1) Mn-Cr
(a-2) Mn-V
(a-3) Mn-CrCo
(a-4) Mn-Al
(a-5) Mn-Re
(b-1) Mn-Cr
(b-2) Mn-V
(b-3) Mn-CrCo
(b-4) Mn-Al
(b-5) Mn-Re
INTEGRATED INTENSITY (arbitrary unit)
Mn 1 2 3 4 5 6
Mn 1 2 3 4 5 6 7
IMPURITY CONCENTRATION (at.%)
(a) SITE I
(b) SITE II

Fig. 10

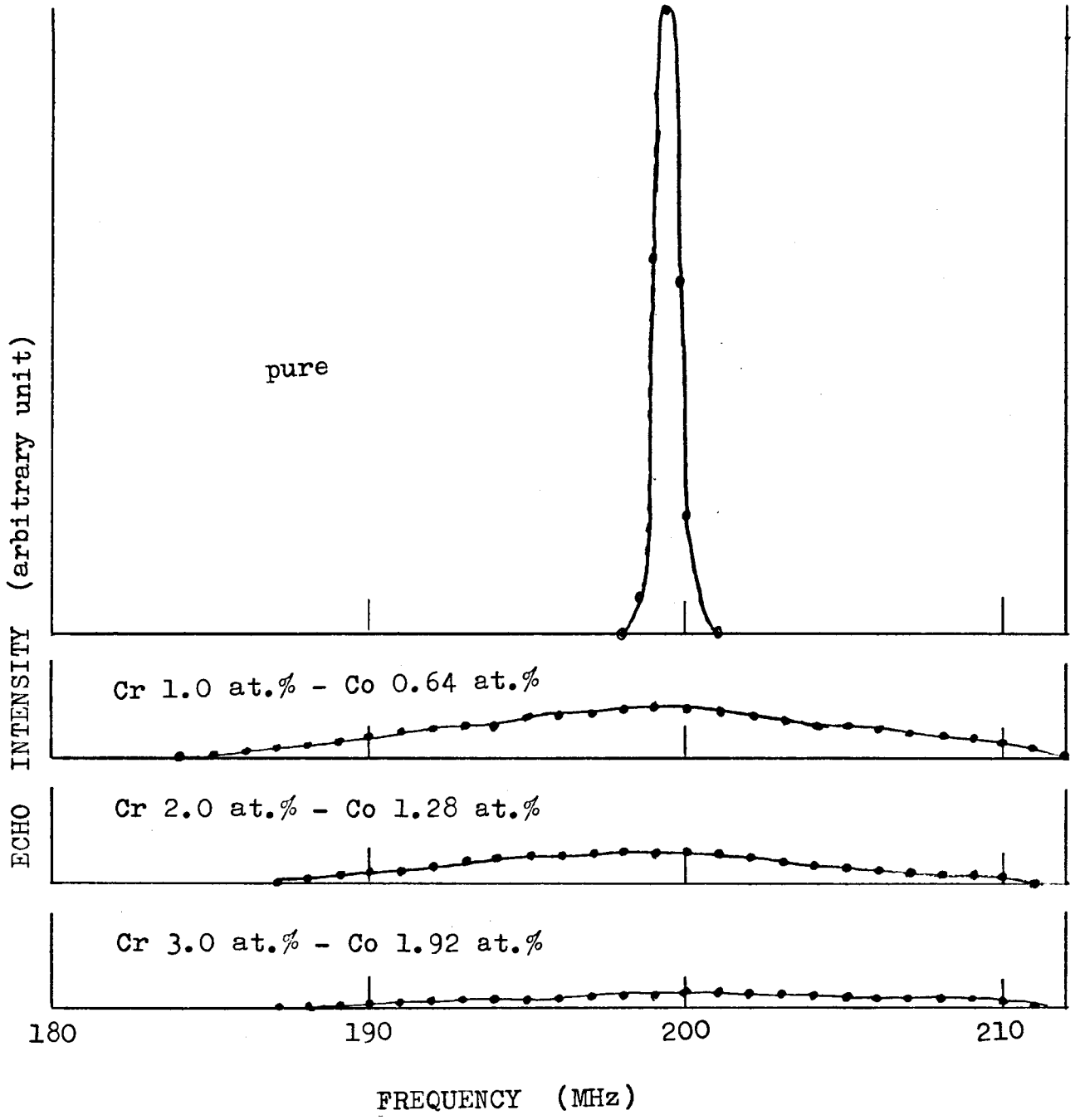
pure
Cr 1.0 at.% - Co 0.64 at.%
Cr 2.0 at.% - Co 1.28 at.%
Cr 3.0 at.% - Co 1.92 at.%
ECHO INTENSITY (arbitrary unit)
180
190
200
210
FREQUENCY (MHz)

Fig. 11

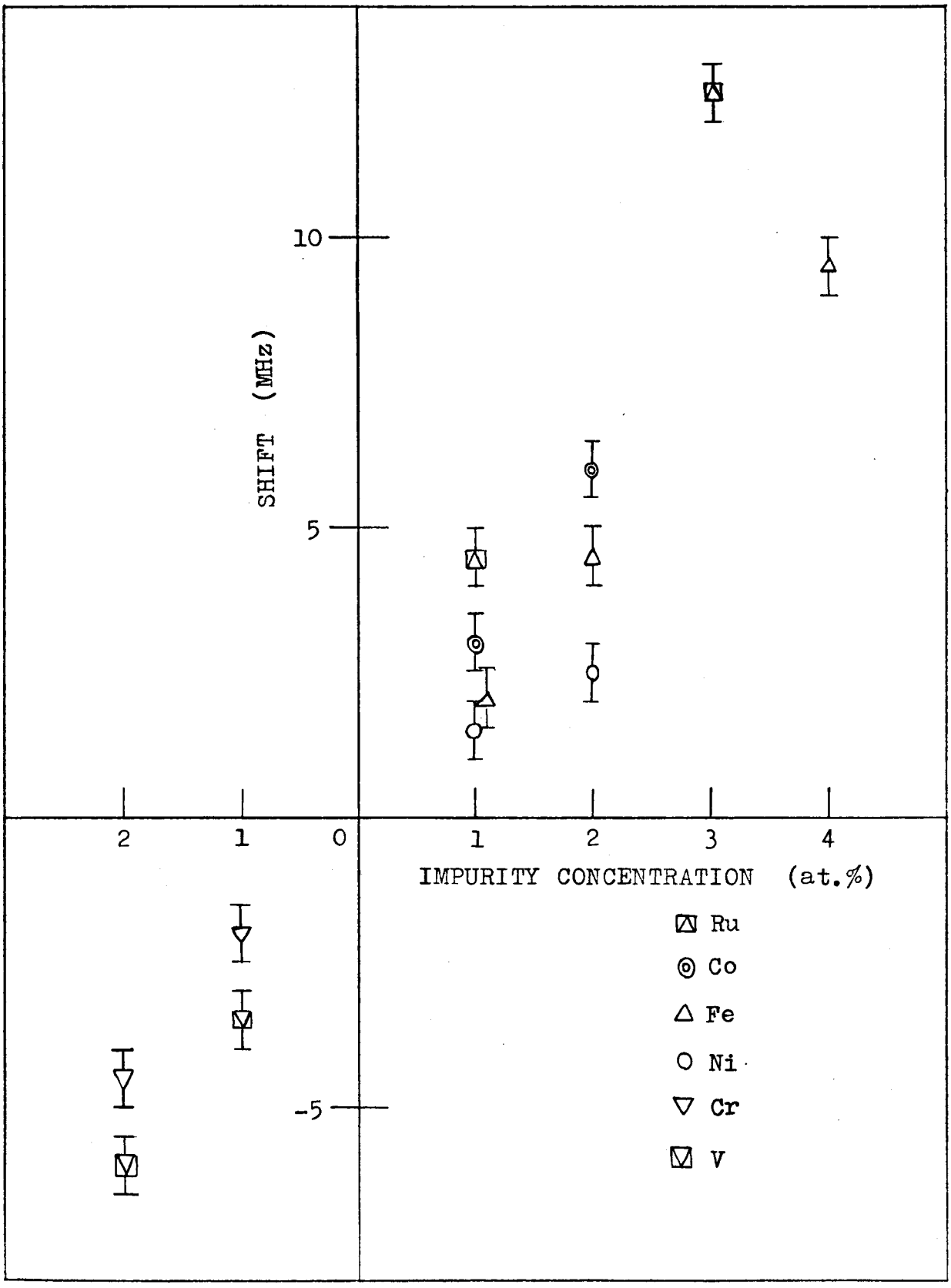
10
5
-5
SHIFT (MHz)
2
1
0
1
2
3
4
IMPURITY CONCENTRATION (at.%)
Ru
Co
Fe
Ni
Cr
V

Fig. 12

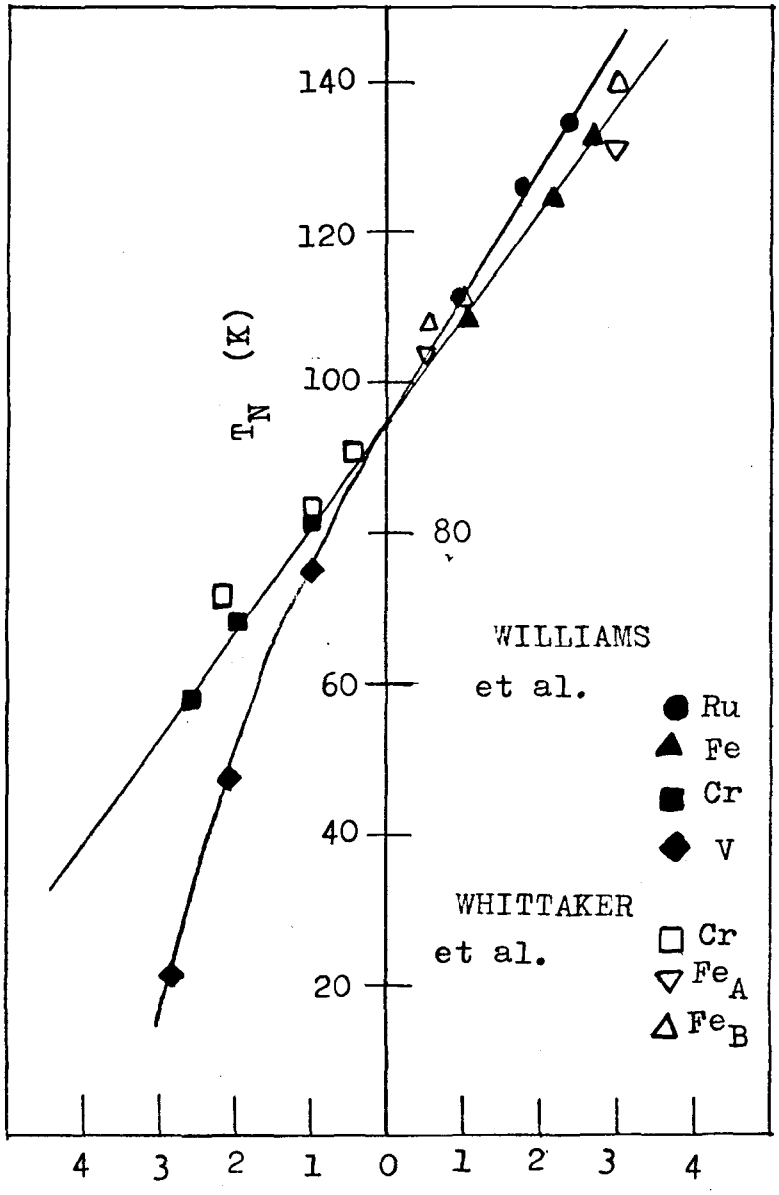
140
120
100
80
60
40
20
T_N (K)
WILLIAMS
et al.
Ru
Fe
Cr
V
WHITTAKER
et al.
Cr
Fe_A
Fe_B
4 3 2 1 0 1 2 3 4
ATOMIC PERCENT SOLUTE

Fig. 13

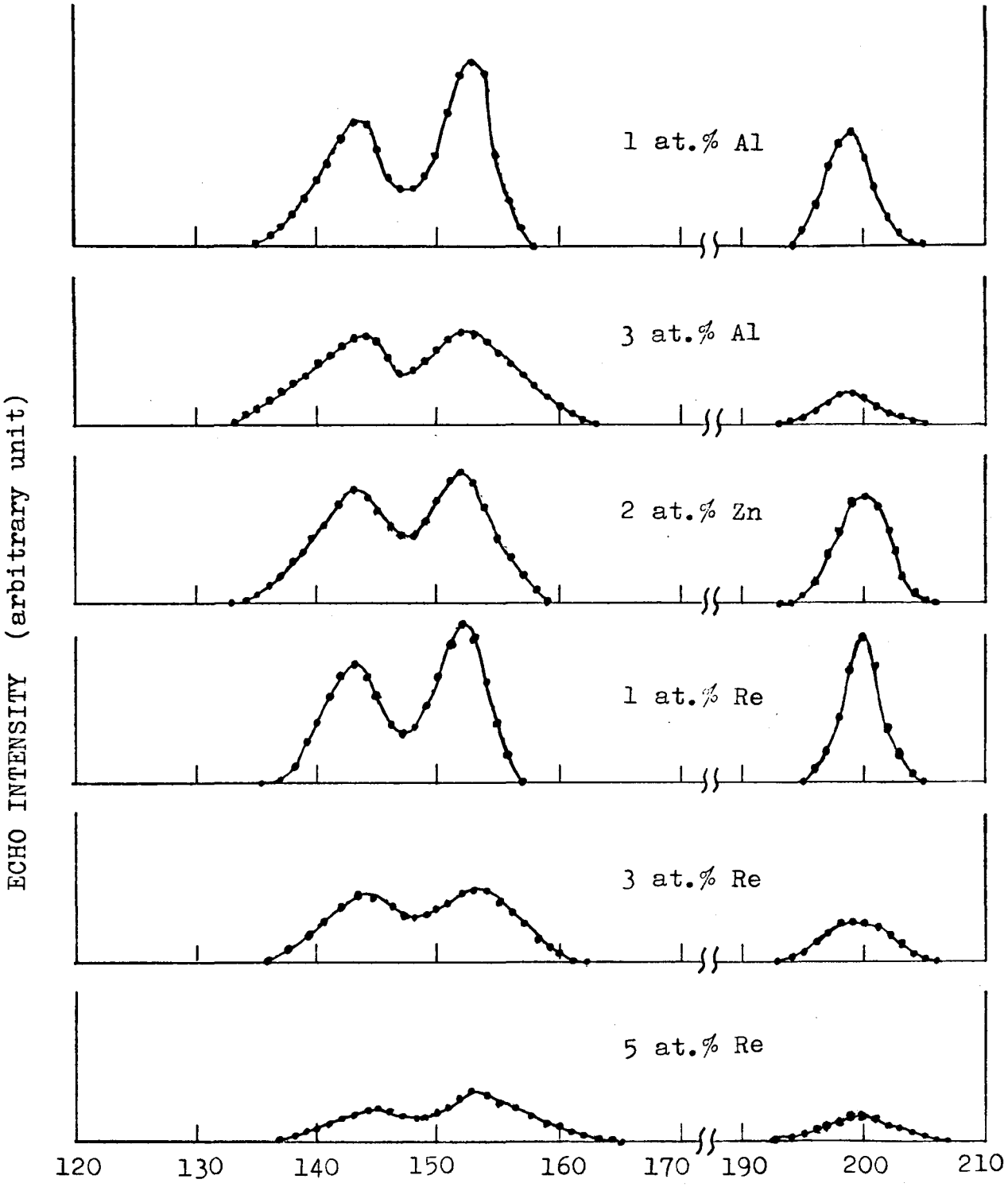
1 at.% Al
3 at.% Al
2 at.% Zn
1 at.% Re
3 at.% Re
5 at.% Re
ECHO INTENSITY (arbitrary unit)
120
130
140
150
160
170
190
200
210
FREQUENCY (MHz)

Fig. 14

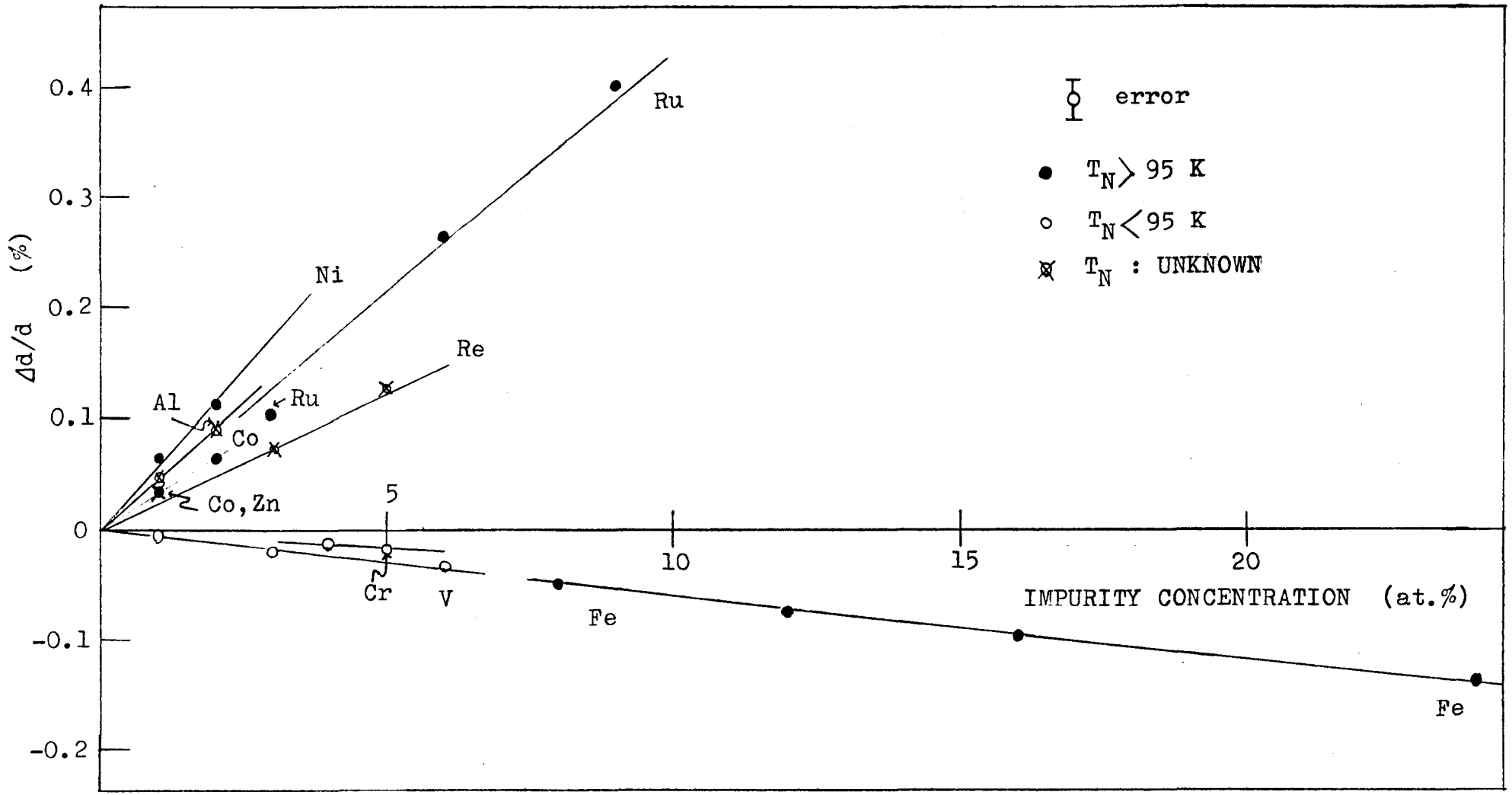
0.4
0.3
0.2
0.1
0
-0.1
-0.2
Δd/d (%)
Ru
Ni
Re
Al
Ru
Co
Co, Zn
Cr
V
Fe
Fe
5
10
15
20
IMPURITY CONCENTRATION (at.%)
error
T_N > 95 K
T_N < 95 K
T_N : UNKNOWN

Fig. 15

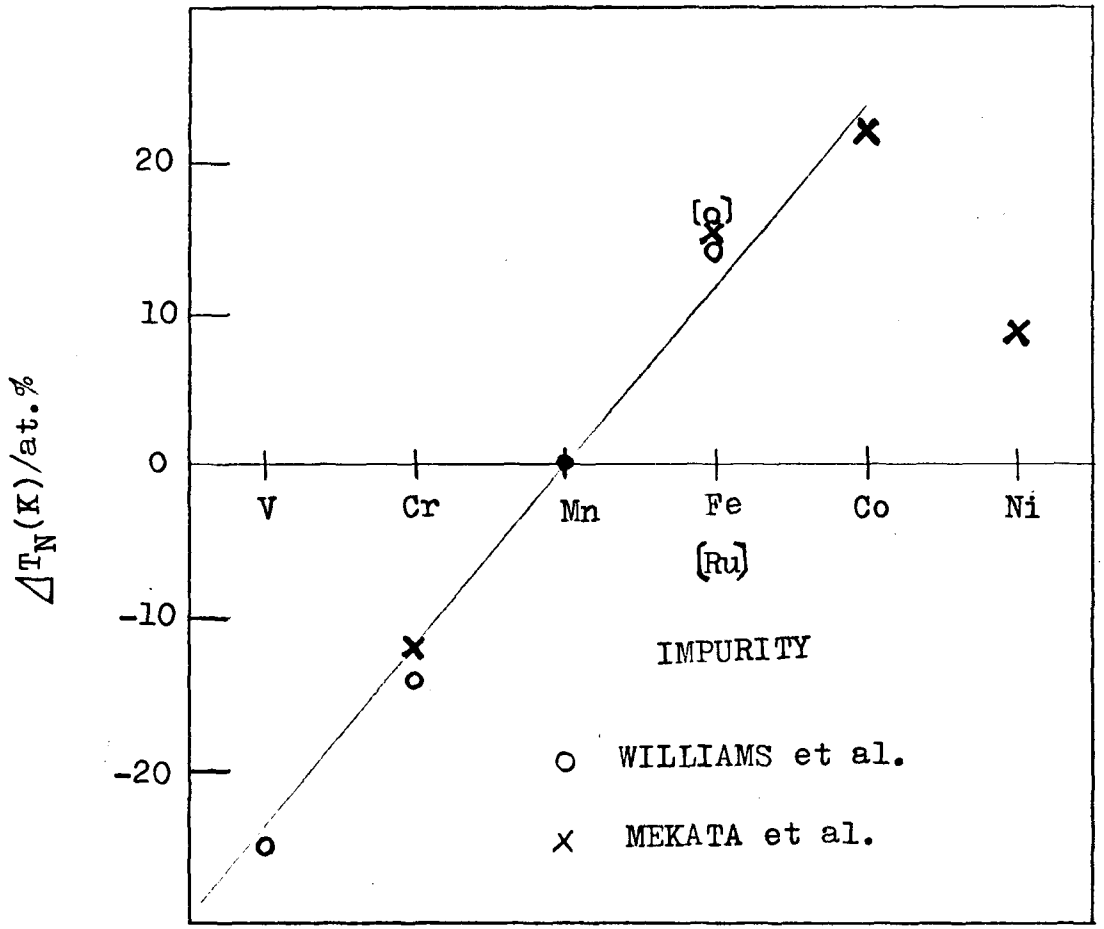
20
10
0
-10
-20
ΔT_N(K)/at.%
V
Cr
Mn
Fe
Co
Ni
(Ru)
IMPURITY
WILLIAMS et al.
MEKATA et al.

Fig. 16

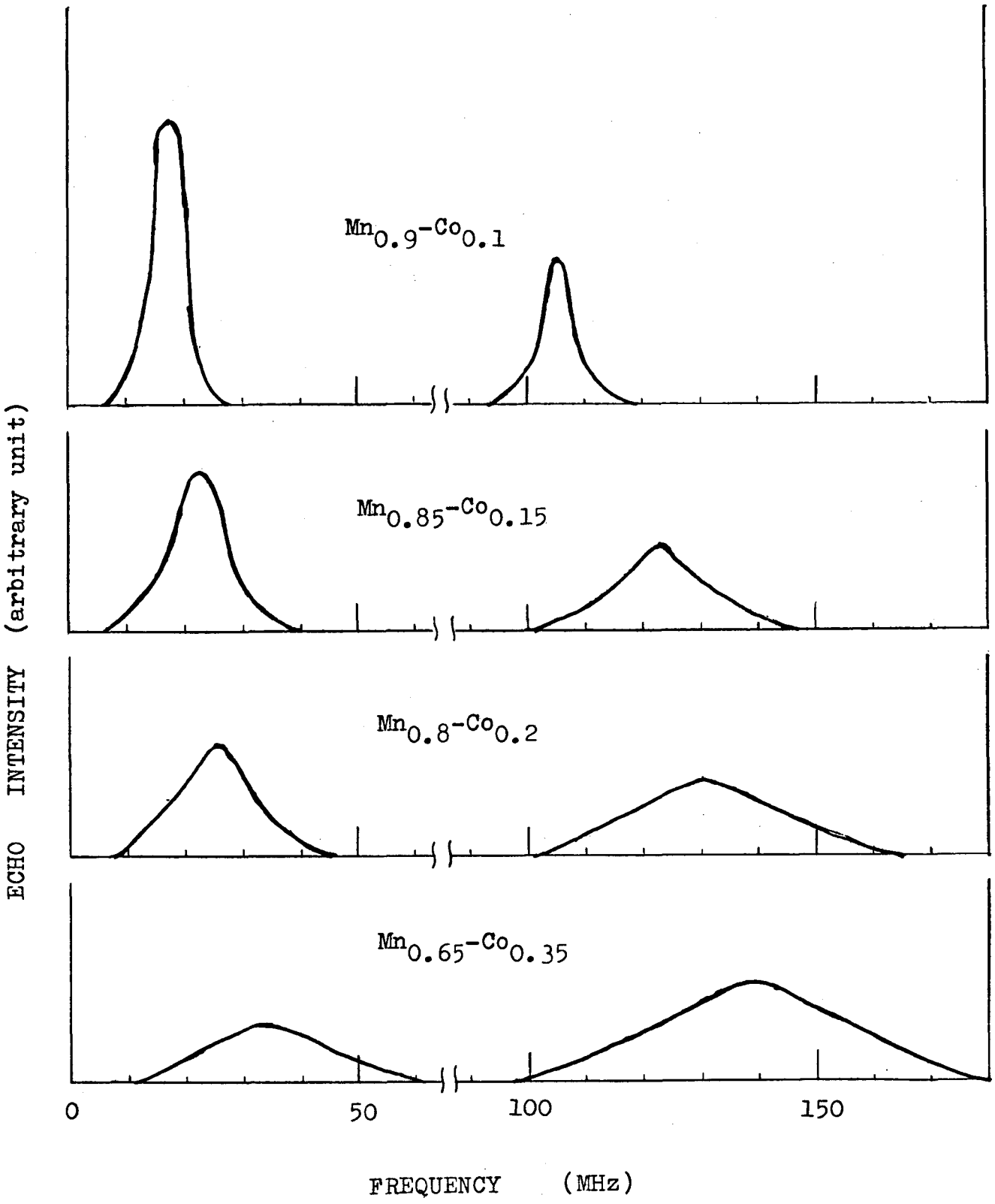
$Mn_{0.9}$-$Co_{0.1}$
$Mn_{0.85}$-$Co_{0.15}$
$Mn_{0.8}$-$Co_{0.2}$
$Mn_{0.65}$-$Co_{0.35}$
ECHO INTENSITY (arbitrary unit)
0
50
100
150
FREQUENCY (MHz)

Fig. 17

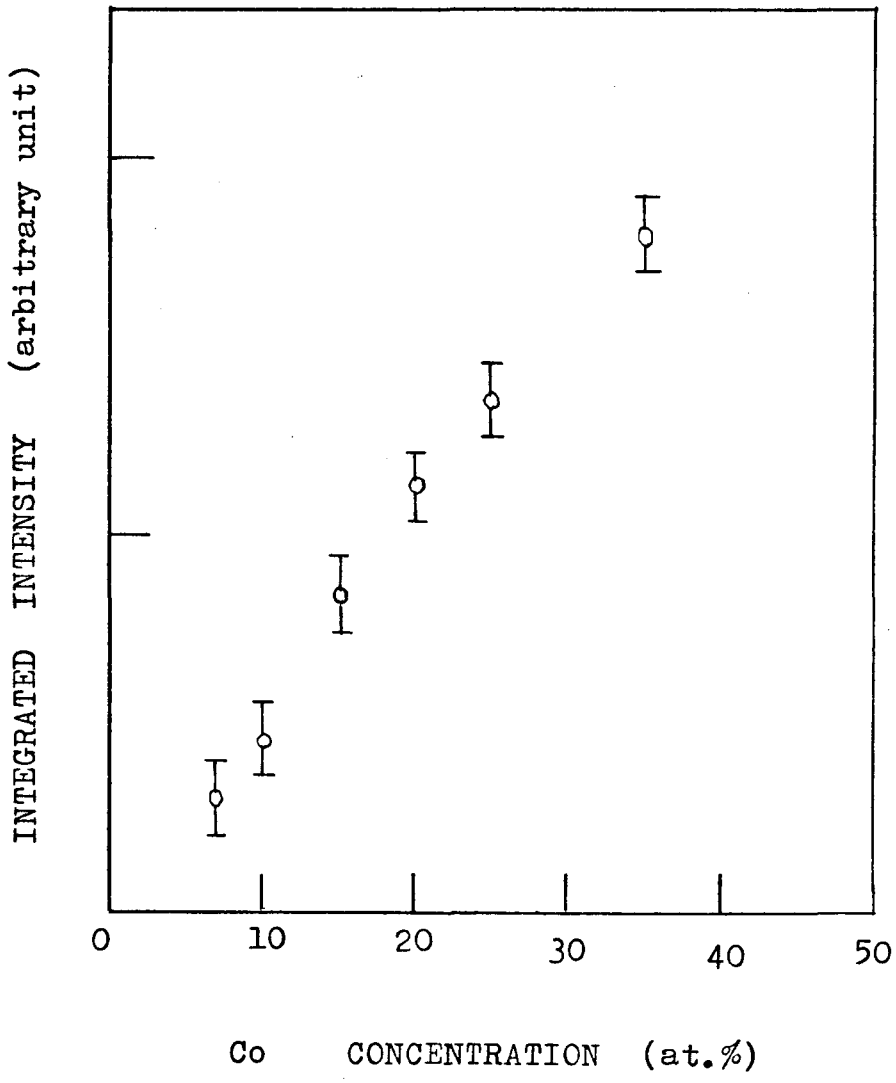
INTEGRATED INTENSITY (arbitrary unit)
0
10
20
30
40
50
Co CONCENTRATION (at.%)

Fig. 18

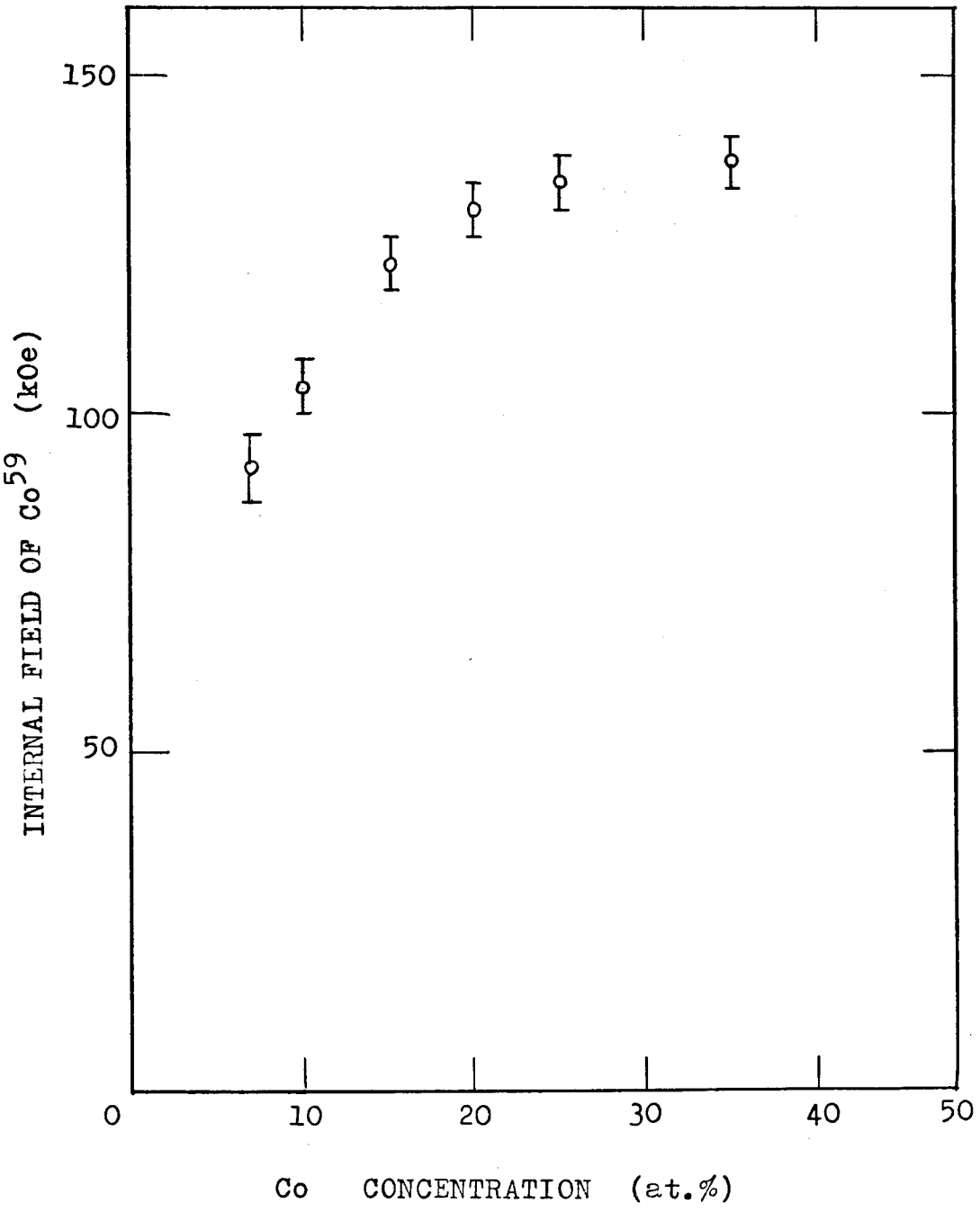
150
100
50
0
10
20
30
40
50
INTERNAL FIELD OF Co^{59} (kOe)
Co CONCENTRATION (at.%)

Fig. 19

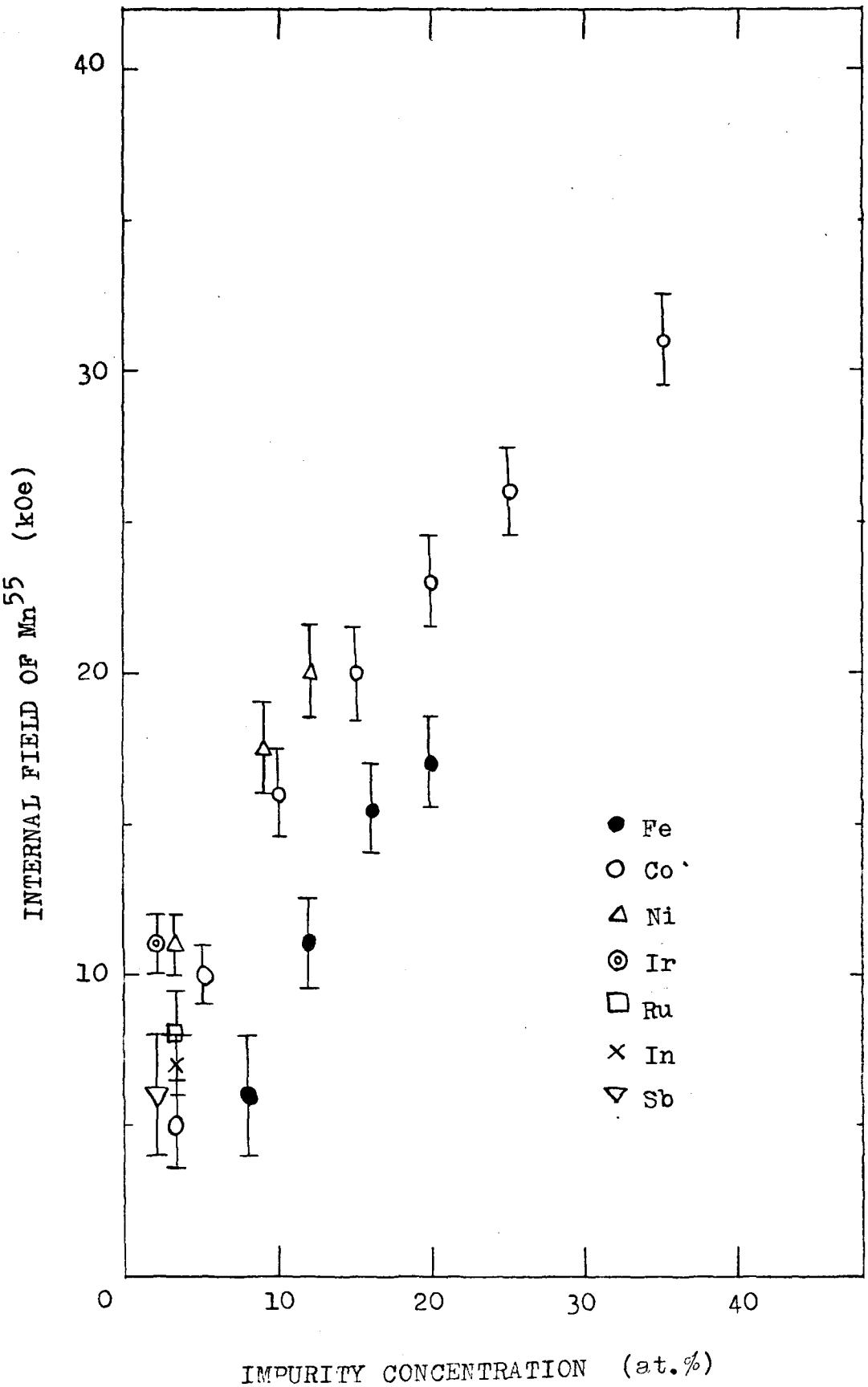
INTERNAL FIELD OF Mn^{55} (kOe)
IMPURITY CONCENTRATION (at.%)
0
10
20
30
40
Fe
Co
Ni
Ir
Ru
In
Sb

Fig. 20

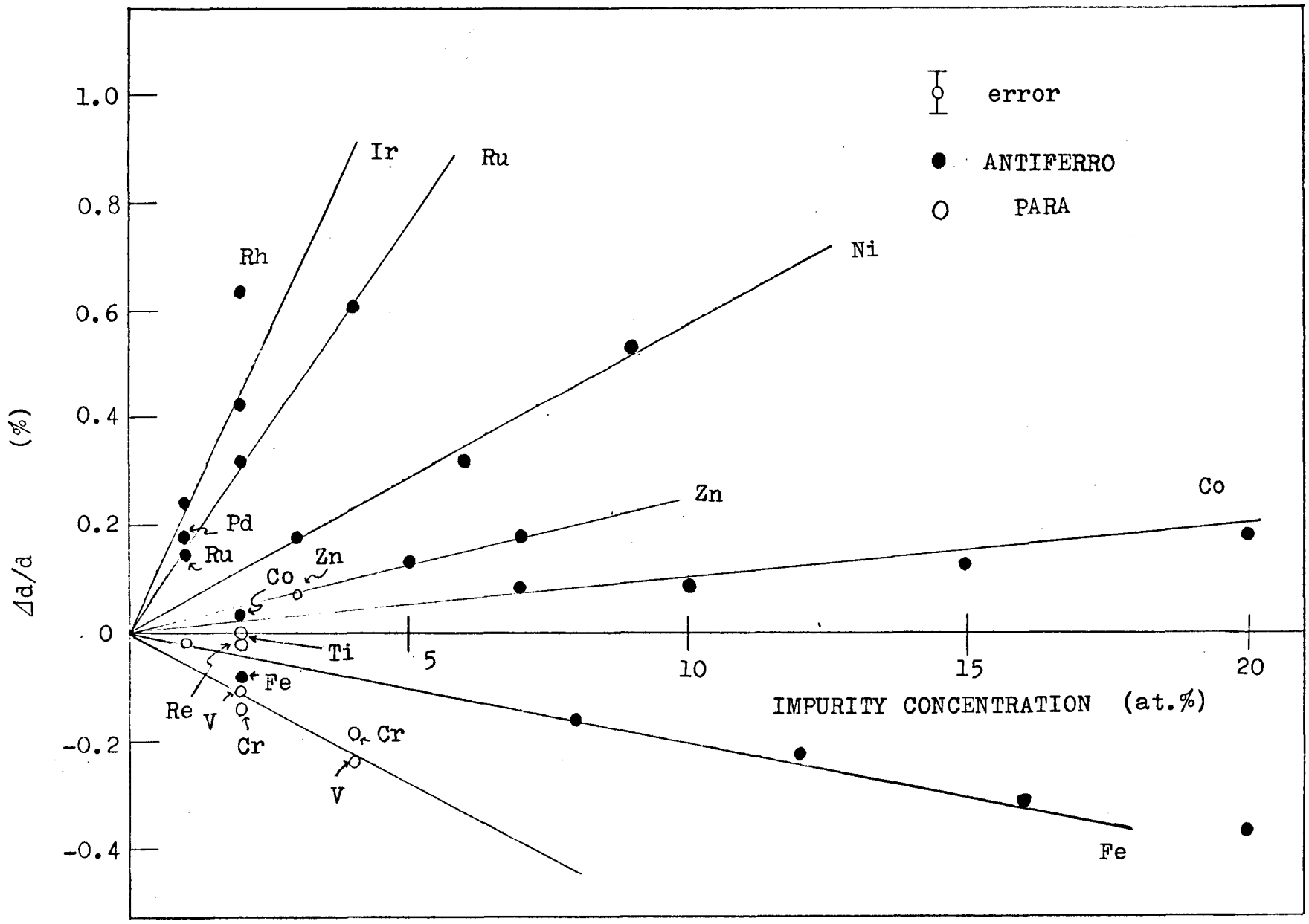
1.0
0.8
0.6
0.4
0.2
0
-0.2
-0.4
Δd/d (%)
error
ANTIFERRO
PARA
Ir
Ru
Rh
Ni
Zn
Co
Pd
Ru
Zn
Co
Ti
Fe
Re
V
Cr
Cr
V
Fe
5
10
15
20
IMPURITY CONCENTRATION (at.%)

Fig. 21

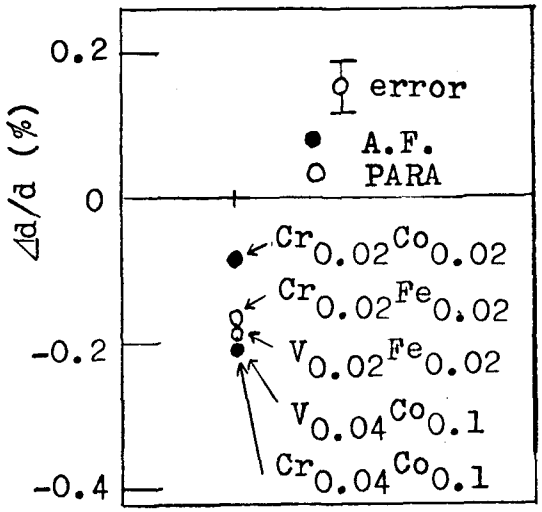
0.2
0
-0.2
-0.4
Δd/d (%)
error
A.F.
PARA
Cr0.02Co0.02
Cr0.02Fe0.02
V0.02Fe0.02
V0.04Co0.1
Cr0.04Co0.1

Fig. 22

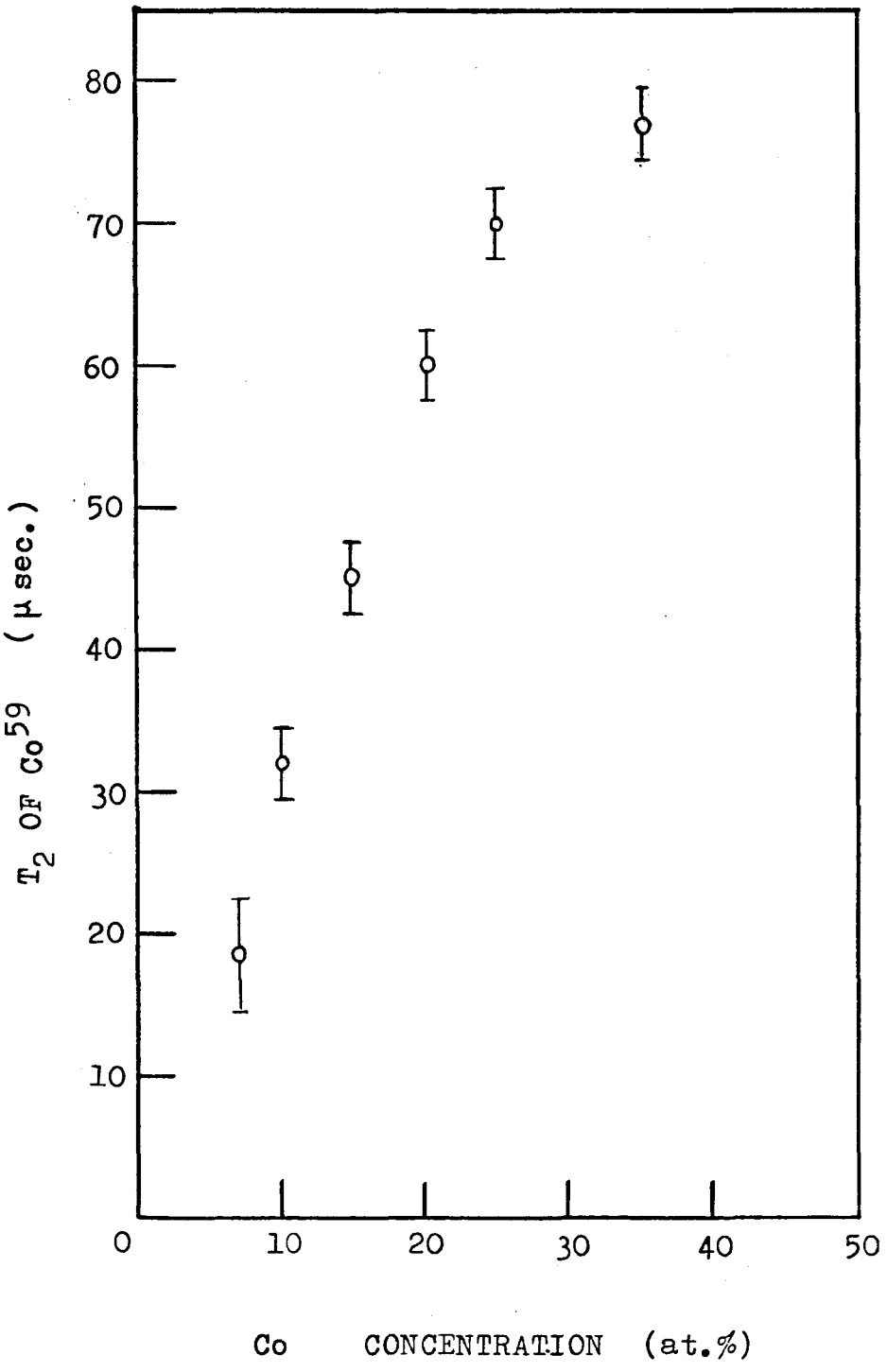
80
70
60
50
40
30
20
10
0
10
20
30
40
50
T_2 OF Co^{59} (μ sec.)
Co CONCENTRATION (at.%)

Fig. 23

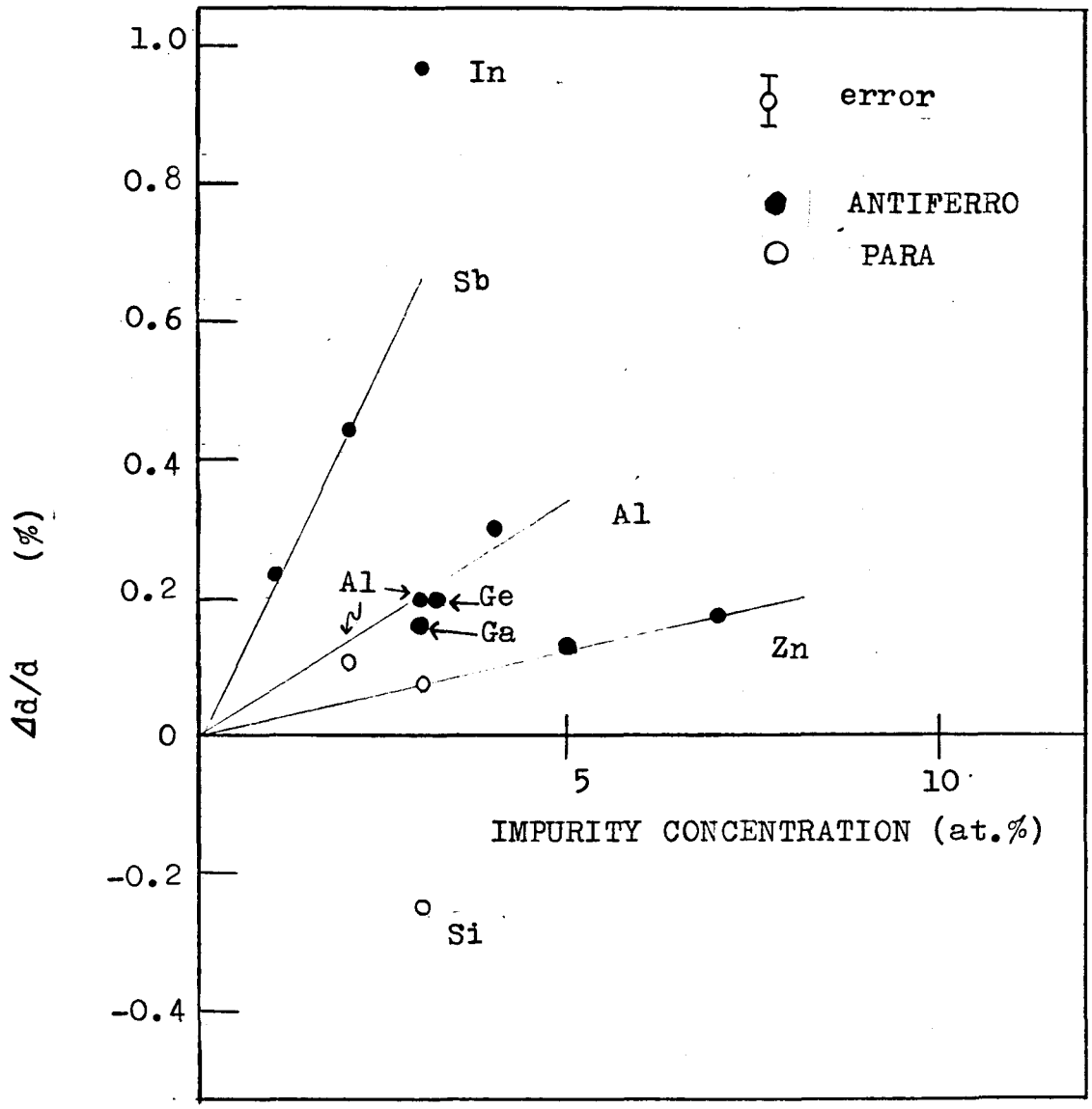
1.0
0.8
0.6
0.4
0.2
0
-0.2
-0.4
Δd/d (%)
In
Sb
Al
Al
Ge
Ga
Zn
Si
error
ANTIFERRO
PARA
5
10
IMPURITY CONCENTRATION (at.%)

Fig. 24

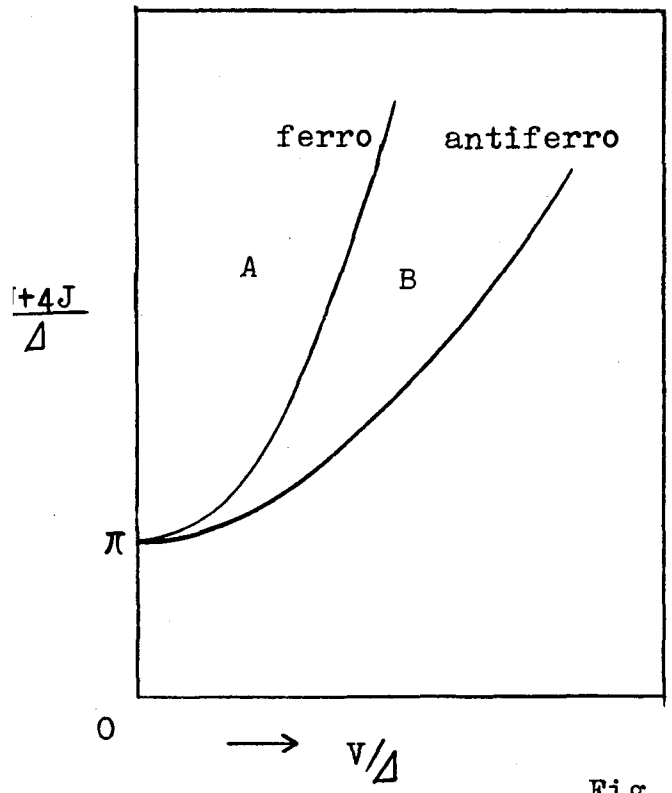

Fig. 25